Joule

CellPress

Article

Computational Screening of Cathode Coatings for Solid-State Batteries

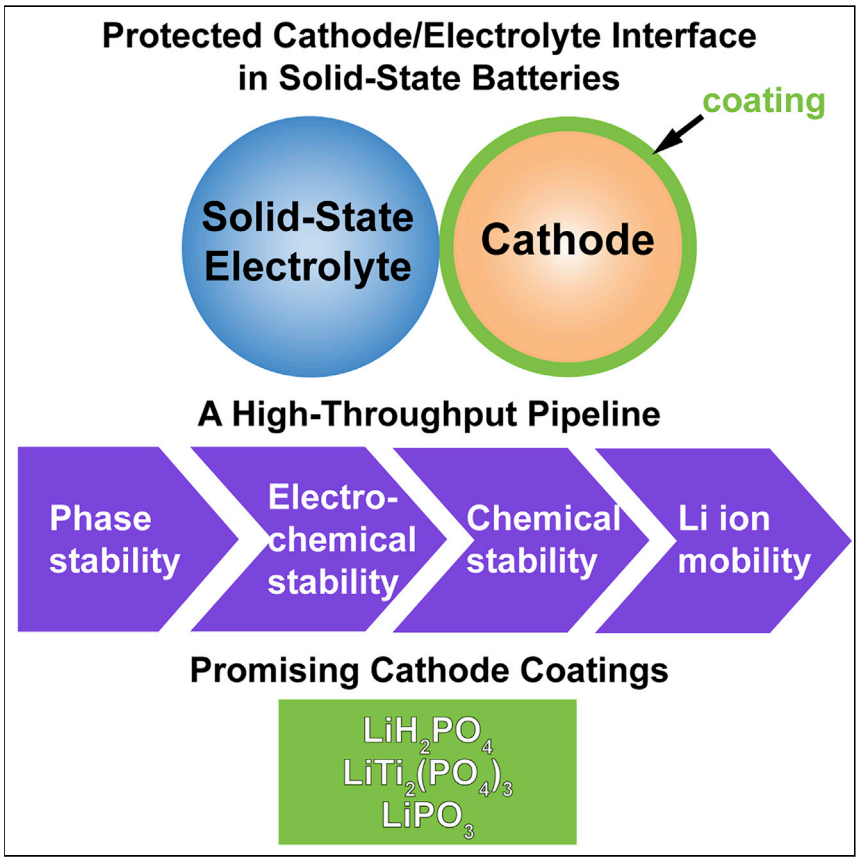

Solid-state batteries are considered the next generation of batteries, but they still suffer from high interfacial resistance. One strategy to mitigate the problem is to use coating. We performed a computational screening to find promising cathode coating compositions. Polyanionic oxides are highlighted for good overall characteristics, and LiH_2PO_4, $LiTi_2(PO_4)_3$, and $LiPO_3$ are particularly appealing candidates. Furthermore, factors including oxygen bond covalency and Li content are identified to affect oxidation stability of polyanionic oxide coatings.

Yihan Xiao, Lincoln J. Miara, Yan Wang, Gerbrand Ceder

gceder@berkeley.edu

HIGHLIGHTS

High-throughput screening of cathode coatings for solid-state batteries

Polyanionic oxides are proposed as promising cathode coatings

Several lithium borates exhibit excellent (electro)chemical stability

Li content and oxygen bonding covalency affect stability of polyanionic oxides

Xiao et al., Joule 3, 1–24
May 15, 2019 Published by Elsevier Inc.
https://doi.org/10.1016/j.joule.2019.02.006

Please cite this article in press as: Xiao et al., Computational Screening of Cathode Coatings for Solid-State Batteries, Joule (2019), https://doi.org/10.1016/j.joule.2019.02.006

Joule

CellPress

Article

Computational Screening of Cathode Coatings for Solid-State Batteries

Yihan Xiao,[1,2] Lincoln J. Miara,[3] Yan Wang,[3] and Gerbrand Ceder[1,2,4,*]

SUMMARY

Solid-state batteries are on the roadmap for commercialization as the next generation of batteries because of their potential for improved safety, power density, and energy density compared with conventional Li-ion batteries. However, the interfacial reactivity and resulting resistance between the cathode and solid-state electrolyte (SSE) lead to deterioration of cell performance. Although reduction of the cathode/SSE interfacial impedance can be achieved using cathode coatings, optimizing their compositions remains a challenge. In this work, we employ a computational framework to evaluate and screen Li-containing materials as cathode coatings, focusing on their phase stability, electrochemical and chemical stability, and ionic conductivity. From this tiered screening, polyanionic oxide coatings were identified as exhibiting optimal properties, with LiH_2PO_4, $LiTi_2(PO_4)_3$, and $LiPO_3$ being particularly appealing candidates. Some lithium borates exhibiting excellent (electro)chemical stability at various interfaces are also highlighted. These results highlight the promise of using optimized polyanionic materials as cathode coatings for solid-state batteries.

INTRODUCTION

Li-ion battery technology has become indispensable in applications ranging from portable electronics to electric vehicles to grid-scale energy storage. However, commercial Li-ion batteries that use organic liquid electrolytes suffer from problems of flammability, low ion selectivity, limited electrochemical stability, and poor stability of the solid-electrolyte interphase (SEI) against Li metal.[1] Solid-state batteries (SSBs) show potential to mitigate these issues by replacing the organic liquid electrolyte with an inorganic solid-state electrolyte (SSE). To avoid compromising the high ionic conductivity (> 1 mS/cm) of liquid electrolytes, solid Li-ion conductors with comparable ionic conductivities are highly desirable. To date, several families of Li-ion conductors that exhibit room-temperature ionic conductivity rivaling that of liquid electrolytes have been discovered.[2] Most of these inorganic SSEs fall into two categories: (1) oxide-based electrolytes including Li garnets[3–5] and Na superionic conductor (NASICON)-type materials[6–10] and (2) sulfide-based electrolytes such as Li_2S-P_2S_5 glass[11] and the glass-ceramics[12] and $Li_{10}GeP_2S_{12}$ (LGPS) and its computationally predicted derivatives with LGPS-type structures.[13–18] Bulk ionic conductivities at room temperature (σ_{RT}) of ~1 mS/cm to greater than 10 mS/cm have been achieved in both categories.[13,17,19]

Nevertheless, the power density, rate capacity, and capacity retention of SSBs employing these superionic conductors remain poor, impeding their ultimate commercial usage.[20,21] These poor properties reflect the high resistance at the electrode/SSE interfaces, which grows upon cycling. Experimental studies of electrode/SSE

Context & Scale

The flammability of organic liquid electrolytes in Li-ion batteries is a serious safety risk. Solid-state batteries (SSBs) replace the liquid with an inorganic solid, dramatically improving the safety. Unfortunately, solid-solid contacts at the cathode/electrolyte interface are often unstable, leading to high interfacial impedance that grows during operation. Buffering this interface with another layer effectively improves stability; however, optimized buffer materials have not been found by previous research. This work develops and uses a computational framework to screen a wide range of chemistries for use as buffer layers between oxide cathodes and sulfide solid electrolytes and identifies the key factors such as Li content and oxygen bonding covalency that affect the stability of these materials. Many of these materials are polyanionic oxides that substantially outperform conventional oxide buffers. Our work provides guidance for material selection for the next-generation SSBs.

Please cite this article in press as: Xiao et al., Computational Screening of Cathode Coatings for Solid-State Batteries, Joule (2019), https://doi.org/10.1016/j.joule.2019.02.006

interfaces have revealed possible causes for the interfacial resistance: (1) mutual diffusion and interfacial reactions between the SSE and the electrode,[22,23] (2) electrochemical decomposition of the SSE at the SSE/electrode and the SSE/carbon interfaces during cell cycling,[24–27] and (3) poor contact between the SSE and the electrode due to poor wetting and/or volume change of the electrode during cycling.[24,28] First-principles calculations have demonstrated the lack of thermodynamic stability of LGPS-type SSEs[18,29] and predicted the interfacial reactions occurring at the interfaces between various electrodes and SSEs in SSBs.[30–35] Hence, engineering stable interfaces in SSBs is critical to further improving the cell performance.

To mitigate the interfacial resistance, a buffer layer is often applied to prevent direct contact between the active material and the electrolyte.[28,36] In principle, either the electrode or the electrolyte could be coated to stabilize the electrode/electrolyte interface. A buffer layer has been used in the protected Li electrode in Li-air batteries to prevent the reduction of Ti^{4+} in NASICON-type solid electrolytes by metallic Li.[37] On the cathode side, coating the electrode is usually preferred because coating the SSE would significantly increase the resistance along ion migration pathways.

Oxides used to coat conventional cathode materials have shown varying degrees of effectiveness in SSBs.[21] They include, among others, Li_3PO_4,[38] $LiAlO_2$ and Al_2O_3,[39] $LiTaO_3$,[40] $LiNbO_3$,[20,41,42] $Li_4Ti_5O_{12}$,[36,43] Li_2SiO_3,[22] Li_3BO_3,[44] and Li_2ZrO_3,[45] most of which are metal oxides. Cathode coatings are used to isolate the SSEs from the low Li chemical potentials exerted by the cathode in its highly charged state, thereby preventing their electrochemical self-decomposition. Indeed, most SSEs are not thermodynamically stable at the voltage of many charged cathodes.[30–32] In terms of chemical stability, energy dispersive X-ray (EDX) spectroscopy mapping has shown that cathode coatings can also prevent direct contact between the electrode and the SSE, thus suppressing elemental diffusion and interfacial chemical reactions.[22,42] Recently, computational results have shown that these oxide materials are effective because of their widened electrochemical windows and excellent chemical stability against oxide cathodes compared with those of SSEs.[30–32] Summarizing insights drawn from experimental and computational studies, an ideal cathode coating material should exhibit the following properties: (1) a wide electrochemical window that spans the cathode operating voltage and overlaps with the electrochemical window of the electrolyte (electrochemical stability), (2) limited chemical reactivity with both the electrolyte and the cathode (chemical stability), (3) reasonable Li-ion mobility, and (4) low electronic conductivity (when paired with electrolytes that are unstable at high voltage).

Whereas the experimental approach to finding new coating materials is time consuming and low throughput, computational evaluation of potential coatings based on properties 1–4 can be more efficient. Using a computational approach developed in the previous works[18,29,35] to predict the electrochemical stability and the chemical stability of different interface systems, Zhu et al. proposed several oxides as potential cathode coatings that are chemically similar to the aforementioned oxide coatings, e.g., Li_4TiO_4, Li_2TiO_3, Li_8SiO_6, Li_4SiO_4, Li_5TaO_5, and Li_3TaO_4.[32] In a similar spirit, Aykol et al. performed high-throughput screening of cathode coatings for Li-ion batteries using liquid electrolytes by considering their thermodynamic stability, electrochemical stability, and hydrofluoric acid (HF) reactivity.[46] For SSBs, it is also desirable to consider the chemical compatibility of the coating with both the cathode and the SSE. In addition, the ionic conductivity, an important criterion for coating performance,[44,47] has often been neglected in the

[1]Department of Materials Science and Engineering, University of California Berkeley, Berkeley, CA 94720, USA

[2]Materials Sciences Division, Lawrence Berkeley National Laboratory, Berkeley, CA 94720, USA

[3]Advanced Materials Lab, Samsung Research America, 3 Van de Graaff Drive, Burlington, MA 01803, USA

[4]Lead Contact

*Correspondence: gceder@berkeley.edu

https://doi.org/10.1016/j.joule.2019.02.006

Please cite this article in press as: Xiao et al., Computational Screening of Cathode Coatings for Solid-State Batteries, Joule (2019), https://doi.org/10.1016/j.joule.2019.02.006

computational search for new coatings, presumably because of the high computational cost of ion conductivity predictions with *ab initio* techniques and the difficulty in integrating them with a high-throughput environment.[48,49]

In this work, we conducted a high-throughput search for suitable materials for cathode coatings spanning a very wide range of chemistries. We systematically considered the following aspects of these coating compounds: phase stability, electrochemical stability, chemical stability (with both cathodes and SSEs), and ionic and electronic conductivity. We demonstrate that polyanionic oxide compounds offer the best combination of excellent electrochemical stability and chemical stability without sacrificing the ionic conductivity. The highly covalent bonds between M and oxygen in the many MO_x (M = non-metal elements) polyhedral units lower the energy of the oxygen orbitals, thereby protecting them from oxidation. This effect increases the oxidation stability while also decreasing the chemical reactivity of the polyanionic compounds. Among the polyanionic oxide compounds identified in the high-throughput screening, we specifically highlight the three compounds LiH_2PO_4, $LiTi_2(PO_4)_3$, and $LiPO_3$ as cathode coatings that show great potential for improved performance relative to that of state-of-the-art coatings.

RESULTS

We performed sequential high-throughput screening for coating materials following the flowchart presented in Figure 1. The database used in this study is an internal database of density functional theory (DFT)-computed bulk energies of compounds with crystal structures obtained from the Inorganic Crystal Structure Database (ICSD)[50] as well as those generated by applying data-mined chemical substitutions.[51] This database contains both energetic information, such as the formation energy, and electronic data, such as the Kohn-Sham band gap. As a prerequisite for achieving reasonable Li ionic conductivity, we only considered the 104,082 Li-containing materials in the dataset as potential coating candidates.

Initial Screening

We began the screening by excluding compounds containing radioactive elements. In addition, cathode coatings designed to stabilize SSEs with low oxidation limits must be electronically insulating (property 4); otherwise, the SSE at the SSE/coating interface will still be subjected to the high voltage of the cathode. We used Kohn-Sham band gaps (E_g) determined from DFT calculations as a first-order screening criterion for electronic conductivity for materials. While a low band gap almost certainly leads to some electronic conductivity,[52] even wide-band-gap materials can exhibit electronic transport when point defects in the material create carriers in the valence or conduction bands.[53] As such, electronic conductivity may depend on synthesis and processing conditions and the susceptibility of the compound to create carrier-generating point defects.[53] While the energy of these defects depends to some extent on the band gap, as it contains the energy to create an electron (hole) in the conduction (valence) band, it is certainly possible that wide-band-gap materials become electronically active under certain synthesis and processing conditions. Such an analysis would require calculations of all possible point defects as a function of Fermi level, as is sometimes done for oxides and chalcogenides,[53,54] but would be fairly expensive in this high-throughput screening and further complicated by the amorphous nature of some coating materials.[40]

Thus, to the first-order approximation, materials that are potentially electronically conducting, such as metals and alloys, were also excluded by limiting the Kohn-Sham band

Please cite this article in press as: Xiao et al., Computational Screening of Cathode Coatings for Solid-State Batteries, Joule (2019), https://doi.org/10.1016/j.joule.2019.02.006

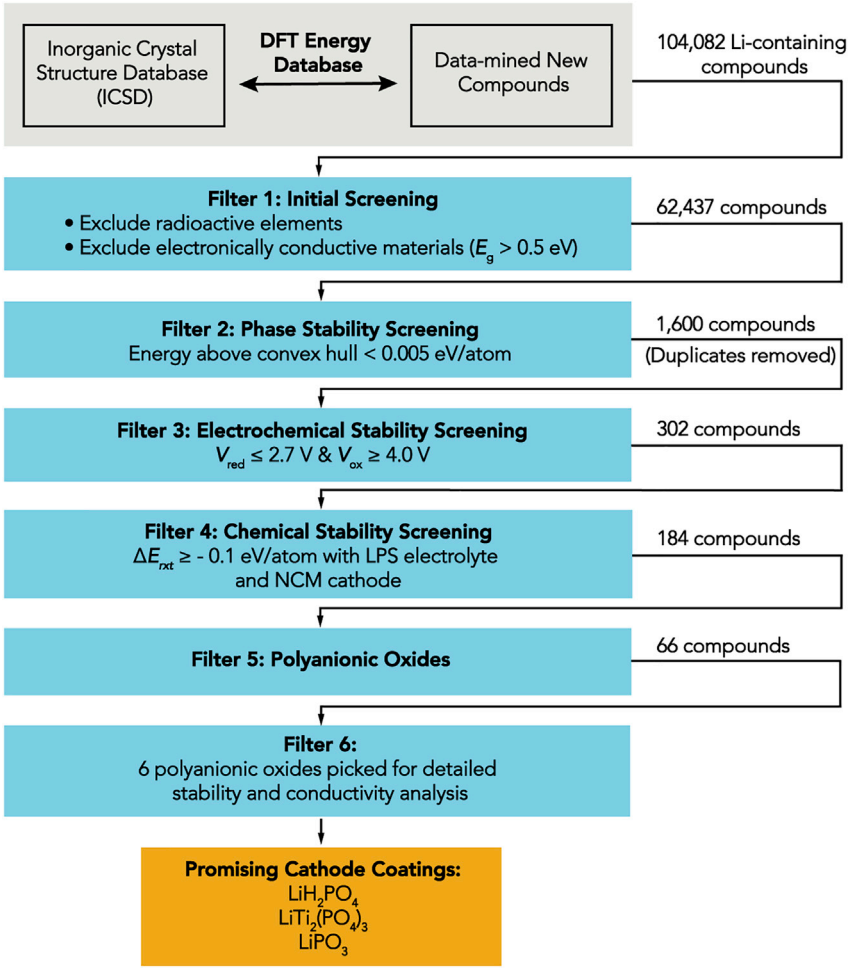

Figure 1. Flowchart Describing the Computational Screening of Cathode-Coating Materials
Following the initial screening, phase stability, electrochemical stability, and chemical stability were used as sequential filters for the high-throughput screening. E_g is the density functional theory (DFT)-calculated Kohn-Sham band gap; V_{red} and V_{ox} are the reduction and oxidation limits of the electrochemical stability window in V versus Li metal, respectively; ΔE_{rxt} is the reaction energy of the material with the cathode or electrolyte in eV/atom; LPS denotes the SSE material Li_3PS_4; and NCM denotes the fully lithiated cathode material $LiNi_{1/3}Co_{1/3}Mn_{1/3}O_2$.

gap to be larger than 0.5 eV. The more than 62,000 compounds that meet these initial screening criteria were then evaluated for their phase stability.

Phase Stability Screening

A good cathode coating is expected to maintain its structural and chemical integrity during the shelf life and the operation of the battery. The phase stability of a material determines both its long-term stability and synthesizability. In this study, we only considered Li-containing materials that are thermodynamically stable (or stable within the DFT or temperature error) against decomposition into other phases. We evaluated the phase stability of a material by building the energy convex hull in the chemical space that includes this material and calculating its energy above this hull (see Experimental Procedures).[30,46] Only materials whose energies are <0.005 eV/atom above the convex hull or exactly on the hull were considered thermodynamically stable (or stable within DFT or temperature error). This phase

Please cite this article in press as: Xiao et al., Computational Screening of Cathode Coatings for Solid-State Batteries, Joule (2019), https://doi.org/10.1016/j.joule.2019.02.006

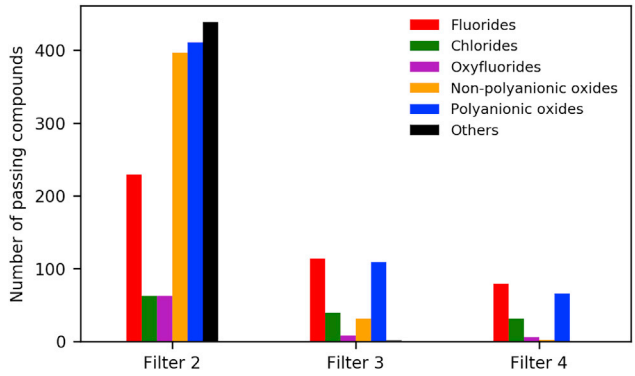

Figure 2. Histogram of Numbers of Compounds for Each Category That Pass Each Filter in the High-Throughput Screening

Red, fluorides; green, chlorides; purple, oxyfluorides; orange, non-polyanionic oxides; blue, polyanionic oxides; black, others. Filter 2, phase stability screening; filter 3, electrochemical stability screening; filter 4, chemical stability screening.

stability filter returned 1,600 compounds with unique compositions for further consideration of the electrochemical stability.

To better understand the composition-property relationship, we categorized materials according to their anion chemistry: fluorides, chlorides, oxyfluorides, oxides, and others (sulfides, nitrides, bromides, iodides, phosphides, etc.). We additionally divided the oxides into polyanionic oxides and non-polyanionic oxides. In this study, polyanionic oxides refer to oxides with "non-metal-oxygen cluster" anion groups, including PO_x^{y-}, SO_4^{2-}, BO_x^{y-}, CO_3^{2-}, AsO_4^{3-}, SeO_4^{2-}, NO_3^-, SiO_3^{2-}, ClO_x^{y-}, BrO_3^-, and IO_x^{y-}. Using this definition, the conventional ternary metal oxide coatings (e.g., $LiAlO_2$, $LiTaO_3$, $LiNbO_3$, $Li_4Ti_5O_{12}$, and Li_2ZrO_3) belong to the non-polyanionic oxides category. Figure 2 and Table 1 summarize the numbers and percentages of compounds for each category of materials that pass the phase stability filter (filter 2), electrochemical stability filter (filter 3), and chemical stability filter (filter 4). As observed in Table 1, greater than 50% of the 1,600 phase-stable materials that pass filter 2 are oxides, implying that oxides have a rich chemical space for property optimization. Note that within the oxide category, there are approximately equal numbers of non-polyanionic oxides (397) and polyanionic oxides (411).

Electrochemical Stability Screening

The Li electrochemical stability window of a material is the voltage range (versus Li metal) in which the material is stable against decomposition by either Li consumption or release. Specifically, the oxidation and reduction limits of the stability window are defined as the voltage limits at which the material begins to be oxidized via Li extraction or reduced via Li insertion, respectively. Thermodynamically, the voltages are obtained from the limits of the Li chemical potential that keeps the grand potential of the material on the convex energy hull.[18,30,55] For example, at the lower chemical potential value of this range (corresponding to higher voltage), the compound will decompose into one or more phases with an overall reduced Li content. Since a significant driving force may be required to form new phases from the compound, some kinetic stabilization beyond the predicted voltage limits may be expected. For example, the overpotential for the oxidation of $Li_7La_3Zr_2O_{12}$ (LLZO) has been shown to be greater than 1 V.[56] The methodology for the electrochemical stability window calculation is described in Experimental Procedures.

Please cite this article in press as: Xiao et al., Computational Screening of Cathode Coatings for Solid-State Batteries, Joule (2019), https://doi.org/10.1016/j.joule.2019.02.006

Table 1. Numbers and Percentages of Compounds for Each Category That Pass Each Filter in High-Throughput Screening

Filter	Fluorides	Chlorides	Oxyfluorides	Non-polyanionic Oxides	Polyanionic Oxides	Others	Total
Filter 2[a]	229 (14.3%)	62 (3.9%)	62 (3.9%)	397 (24.8%)	411 (25.7%)	439 (27.4%)	1,600
Filter 3[b]	114 (37.7%)	39 (12.9%)	8 (2.6%)	31 (10.3%)	109 (36.1%)	1 (0.3%)	302
Filter 4[c]	79 (42.9%)	31 (16.8%)	6 (3.3%)	2 (1.1%)	66 (35.9%)	0 (0.0%)	184

[a]Phase stability screening.
[b]Electrochemical stability screening.
[c]Chemical stability screening.

The operating voltage of modern cathode materials can vary widely from 2.5 to 4.5 V during charge and discharge cycles. For a cathode coating to be effective, the oxidation limits should be high enough for it to be stable at the top of the charge. To allow for some potential kinetic stabilization, we set the criterion for the oxidation limit to be 4.0 V. For the reduction limit, the coating can only be stable with the electrolyte if its electrochemical window overlaps with that of the electrolyte to ensure that there is no driving force for Li transfer between the coating and the electrolyte. Given that the calculated oxidation limits of sulfide electrolytes are typically in the range of 2.2–2.7 V,[30] we set the reduction limit of coatings to be 2.7 V. Therefore, the final stability window criterion used for the electrochemical stability screening was an oxidation limit of $V_{ox} \geq 4.0$ V and a reduction limit of $V_{red} \leq 2.7$ V.

Figure 3A plots the electrochemical stability windows of all 1,600 compounds that pass the phase stability screening. As noted by Richards et al., the oxidation limit of a material is primarily determined by the anion chemistry.[30] Separation of the oxidation limits of materials with different anions is also evident in Figure 3A. Fluorides typically have the highest oxidation limits, followed by chlorides, polyanionic oxides, and non-polyanionic oxides. Compounds in the "Others" category generally have the lowest oxidation limits, below 2.5 V. In Figure 3A, the horizontal dashed line at 4.0 V denotes the oxidation limit minimum in the electrochemical stability window criterion, and the vertical dashed line at 2.7 V denotes the reduction limit maximum. The region shaded in green in the top left corner therefore represents the stability window of interest, which contains 302 compounds. Figure 2 and Table 1 show that almost all the compounds in the "Others" category are eliminated during this round of screening because of their low oxidation limits, consistent with previous findings for sulfides, nitrides, and phosphides.[30] Table 1 also shows that approximately half of the phase-stable fluorides and chlorides meet the electrochemical criterion, which is the highest percentage among all the chemistries. Notably, after this round of screening, the polyanionic oxides (109) outnumber the non-polyanionic oxides (31) because of their higher pass rates (26.5% for polyanionic oxides versus 7.8% for non-polyanionic oxides). It is worth noting that several polyanionic oxide coatings that have been used in cells with liquid electrolyte have oxidation limits exceeding our threshold (e.g., $LiCoPO_4$ (4.19 eV),[57,58] $LiNiPO_4$ (4.22 eV), and [59] $LiTi_2(PO_4)_3$ (4.59 eV)[60]), explaining their reported good performance. The pass rate is 12.9% for oxyfluorides, which is in between the numbers for polyanionic oxides and non-polyanionic oxides. This is because in these compounds with mixed anions, the oxidation limit is determined by the anion with the lowest oxidation limit. Since oxides have lower oxidation limits than those of fluorides, it is expected that the oxidation limits and pass rate of oxyfluorides are similar to those of oxides.

Please cite this article in press as: Xiao et al., Computational Screening of Cathode Coatings for Solid-State Batteries, Joule (2019), https://doi.org/10.1016/j.joule.2019.02.006

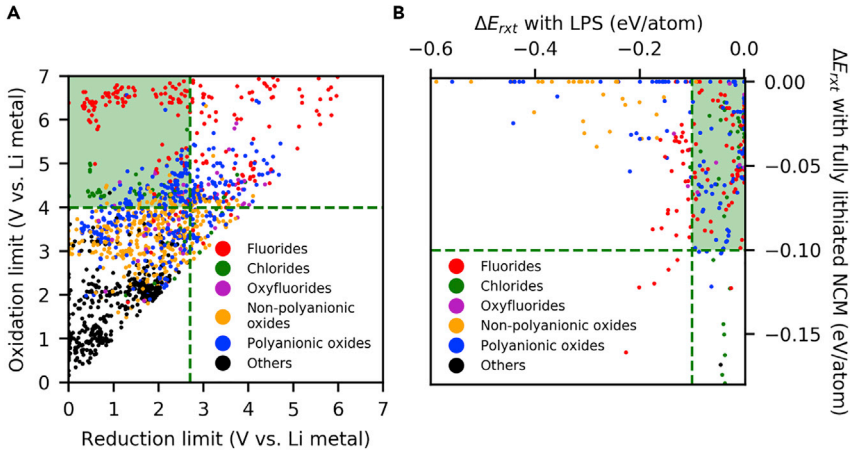

Figure 3. Electrochemical and Chemical Stability Screening Results

Each material is represented by a dot in the graphs. Red, fluorides; green, chlorides; purple, oxyfluorides; orange, non-polyanionic oxides; blue, polyanionic oxides; black, others.

(A) Electrochemical stability windows of 1,600 phase-stable materials.

(B) Chemical reaction energy ΔE_{rxt} with Li_3PS_4 (LPS) and fully lithiated $LiNi_{1/3}Co_{1/3}Mn_{1/3}O_2$ (NCM) for the 302 screened materials enclosed in the green box in Figure 3A. See also Table S1.

Chemical Stability Screening

Next, we considered the chemical stability requirements for cathode coatings. In the absence of a coating, chemical reactions at the interface between the cathode and the SSE have been observed to occur and are accompanied by the interdiffusion of atoms and the formation of ionically insulating phases.[22,23] When a cathode is coated, the cathode/SSE interface is replaced by two new interfaces: the cathode/coating interface and the coating/SSE interface. For a coating to function as designed, it should not only act as a physical barrier that prevents interdiffusion between the SSE and the cathode but also provide two new interfaces that are more stable than the original cathode/SSE interface. For each interface system, we determined the chemical mixing reaction with the most negative reaction energy (ΔE_{rxt}) using DFT-computed energies of the reactants and possible products. The magnitude $|\Delta E_{rxt}|$ was used as an indicator of the chemical reactivity of that interface, with a high $|\Delta E_{rxt}|$ indicating a reactive interfacial system. The methodology used for the chemical mixing energy calculation is described in the Experimental Procedures.[30]

As an example, Figure 3B plots the reaction energy of possible coating materials with Li_3PS_4 (LPS) as the SSE and the reaction energy with fully lithiated $LiNi_{1/3}Co_{1/3}Mn_{1/3}O_2$ (NCM) as the cathode for all 302 materials that pass the electrochemical stability filter (filter 3). This plot is relevant for a coating that would be used to protect LPS from NCM. As observed in Figure 3B, all of the non-polyanionic oxides exhibit limited reactivity ($|\Delta E_{rxt}| < 50$ meV/atom or 4.8 kJ/mol) with NCM; however, over three-quarters of them exhibit large reactivity ($|\Delta E_{rxt}| \geq 200$ meV/atom or 19.3 kJ/mol) with LPS. Greater than 60% of the polyanionic oxides, however, exhibit limited reactivity ($|\Delta E_{rxt}| \leq 100$ meV/atom or 9.6 kJ/mol) with both LPS and NCM. To identify cathode coatings that are chemically compatible with both the electrolyte and the cathode, we set the criterion for chemical reactivity (defined as $|\Delta E_{rxt}|$) of the material to be smaller than 100 meV/atom with both LPS and fully lithiated NCM. This reactivity criterion was used to define the green shaded region in Figure 3B. This region contains 184 compounds, 106 of which were obtained from the ICSD. We provide their compositions, electrochemical windows, and reactivity (with NCM and LPS) in Table S1 for the

Please cite this article in press as: Xiao et al., Computational Screening of Cathode Coatings for Solid-State Batteries, Joule (2019), https://doi.org/10.1016/j.joule.2019.02.006

reader's reference. In Table 1, we see a preference for polyanionic oxides over non-polyanionic oxides even stronger than that observed in the electrochemical-stability-screening round. Concretely, the pass rates are 60.6% for polyanionic oxides versus 6.5% for non-polyanionic oxides. After this round of screening, only two non-polyanionic oxides remain. Interestingly, $LiCoPO_4$ and $LiNiPO_4$ coatings used in cells with organic liquid electrolytes were filtered out because of their high reactivity (~150 meV/atom) with LPS to form transition metal sulfides and lithium phosphates, indicating that they may not be suitable for use in SSBs with sulfide electrolytes.

Down-Selection to Polyanionic Oxides

Fluorides and chlorides are two classes of materials that exhibit exceptional electrochemical stability and chemical stability. As observed in Table 1, together they account for nearly 60% of the 184 compounds passing filter 4. In particular, LiF, LiCl, $LiRbCl_2$, $LiCsCl_2$, and $LiRb_2Cl_3$ have zero reactivity with both fully lithiated NCM and LPS. However, the halides have been less explored than polyanionic oxides in terms of ionic conductivity. Except for one recent report on Li_3YCl_6 with σ_{RT} = ~10^{-4} S/cm,[61] there have only been limited reports on lithium chlorides, with the best room-temperature ionic conductivity reported being approximately 10^{-6} S/cm,[62–64] and no inorganic fluorides as Li-ion conductors were reported to the best of our knowledge. In comparison, numerous polyanionic oxides have been reported to exhibit reasonably high room-temperature ionic conductivity such as NASICON-type phosphates (σ_{RT} = ~10^{-4} S/cm),[9,10,65,66] lithium superionic conductor (LISICON)-type phosphates (σ_{RT} = ~10^{-4} S/cm),[67] and lithium phosphorus oxynitride (LiPON) (σ_{RT} = ~10^{-6} S/cm).[68,69] We decided to focus on polyanionic oxides for further analysis given that (1) some of them are known to be good Li-ion conductors and (2) there are well-known methods to synthesize and apply them as coatings. However, we want to emphasize that halides also have the potential to exhibit comparable stability and ionic conductivity as shown recently by Li_3YCl_6.[61] Table S1 provides a thorough list of the coating candidates that pass the chemical stability filter that includes a wide range of chemistries, including fluorides and chlorides.

Even though we greatly narrowed down the compounds of interest to 66 polyanionic oxides, it remains computationally expensive to study all of these candidates using *ab initio* techniques, especially for dynamic properties such as the Li-ion mobility. We therefore selected six representative compounds from the 66 polyanionic oxides to assess their potential as cathode coatings in detail. These six compounds included the ortho-phosphates LiH_2PO_4 and $LiTi_2(PO_4)_3$, meta-phosphates $LiPO_3$, $LiLa(PO_3)_4$, and $LiCs(PO_3)_2$, and borate $LiBa(B_3O_5)_3$. These candidates are among the polyanionic oxides with the highest oxidation limits (≥4.5 V) in Table S1.

Stability of Six Polyanionic Oxides

The electrochemical stability windows for the six polyanionic oxides are plotted as a bar graph in Figure 4. For comparison, we also plotted the electrochemical stability windows of common thiophosphate electrolytes: argyrodite Li_6PS_5Cl (LPSCl), LGPS, the glass-ceramic LPS, and garnet-type LLZO and the ternary non-polyanionic coatings Li_2ZrO_3,[45] $LiNbO_3$,[20] and $LiTaO_3$.[40] Consistent with the poor electrochemical stability of sulfides in general, the three thiophosphates exhibit low oxidation limits <2.5 V.[25] The oxide LLZO has a wider stability window with an oxidation limit of 2.9 V, which is still too low to be paired with high-voltage cathodes. Indeed, a recent experimental study showed that the apparent oxidation limit of LLZO is approximately 4.0 V,[56] indicating that slow oxidation kinetics may protect the material

Please cite this article in press as: Xiao et al., Computational Screening of Cathode Coatings for Solid-State Batteries, Joule (2019), https://doi.org/10.1016/j.joule.2019.02.006

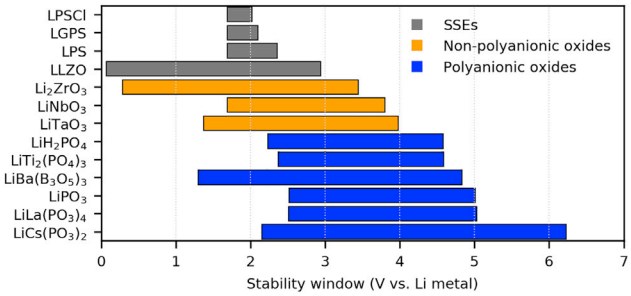

Figure 4. Electrochemical Stability Windows of Common Thiophosphate and Oxide Solid-State Electrolytes (Gray), Non-polyanionic Oxide Coatings (Orange), and Polyanionic Oxides (Blue)

somewhat above its thermodynamic limit but not enough for it to function in battery systems for which the voltage is above 4.0 V. Thus, protection of LLZO at high voltage remains necessary. The three ternary metal-oxide-coating materials listed in Figure 4 exhibit improved oxidation stability (3.4–4.0 V) as compared to both thiophosphate and oxide electrolytes, which explains their previously reported good performance.[20,40–42,45] In comparison, the polyanionic oxides listed in Figure 4 offer substantially higher oxidation limits ($\geq$4.5 V) than those of non-polyanionic oxide coatings. For example, the ortho-phosphate $LiTi_2(PO_4)_3$ exhibits an oxidation limit of 4.6 V and all three meta-phosphates are stable at 5 V or higher, making it possible to pair them with extremely high-voltage cathodes such as $LiNi_{0.5}Mn_{1.5}O_4$ ($\sim$4.7 V).[70,71]

To examine the chemical reactivity of the down-selected coatings with cathodes and electrolytes, we use the color-mapped cells representing the reaction energies ΔE_{rxt} in Figure 5 for the various interfaces: fully lithiated cathode/coating, fully lithiated cathode/SSE, and SSE/coating. The SSEs and coatings are the same as those in Figure 4, and the cathodes evaluated are the commonly used oxide cathodes NCM, $LiCoO_2$ (LCO), $LiMn_2O_4$ (LMO), and $LiFePO_4$ (LFPO). The exact reaction energies and products are listed in Tables S2, S4, and S5, respectively. To determine the compatibility of the interfaces involving cathodes at different states of charge, we repeated the procedure for half-lithiated cathodes, and the reaction energies and products for the most favorable reactions are tabulated in Tables S3 and S4, respectively.

As observed in Figure 5, all the thiophosphate electrolytes (LPSCl, LGPS, and LPS) react strongly with all the cathodes except for LFPO, as indicated by the red colors and very negative reaction energies in Table S2. Specifically, the LPS/NCM interface of interest has a reactivity $|\Delta E_{rxt}|$ as high as 422 meV/atom (40.7 kJ/mol). This high reactivity is even more pronounced at the half-lithiated cathode/SSE interface (Table S3). As noted in previous studies,[30,33] the high reactivity between the oxide cathode and thiophosphates originates in part from the strong tendency to exchange O and S between the SSE and cathode and form PO_4^{3-} groups (as in Li_3PO_4) and transition-metal sulfides, and the formation of P-O_x species was indeed detected experimentally at the NCM/LPS interface.[24] The exchange of O-S is energetically favorable because the bond dissociation energy is much larger for a P-O bond (597 kJ/mol) than for a P-S bond (346 kJ/mol), while the bond dissociation energy difference is small for transition metal-O (e.g., Co-O: 368 kJ/mol) and transition metal-S bonds (e.g., Co-S: 343 kJ/mol).[72] However, in the LFPO cathode, phosphorus is already fully bonded with O atoms, leading to a lower reactivity of LFPO with thiophosphates. Although some modeling results have been used to argue

Please cite this article in press as: Xiao et al., Computational Screening of Cathode Coatings for Solid-State Batteries, Joule (2019), https://doi.org/10.1016/j.joule.2019.02.006

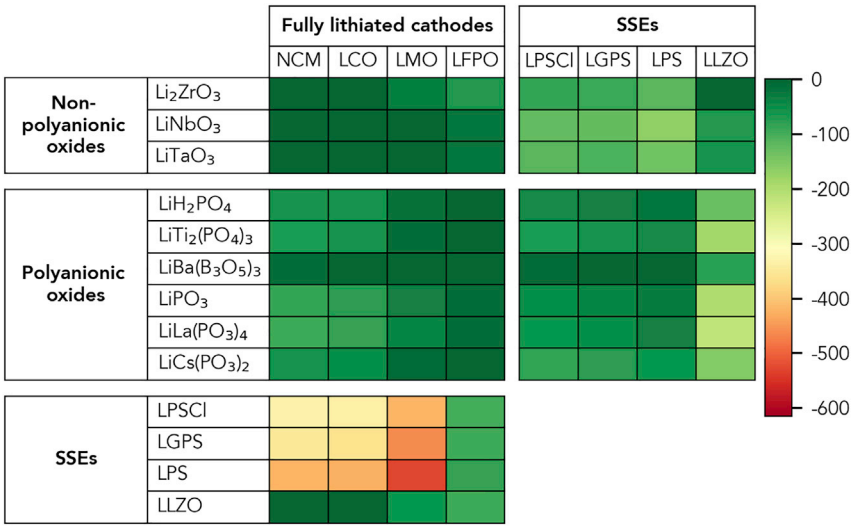

Figure 5. Reaction Energies ΔE_{rxt} at Fully Lithiated Cathode/SSE, Fully Lithiated Cathode/Coating, and Coating/SSE Interfaces in meV/atom

The specific values for ΔE_{rxt} are provided in Table S2. Each cell is mapped to a color from green to red according to the color bar on the right, with the dark green color denoting low chemical reactivity and the dark red color denoting high chemical reactivity. See also Tables S2–S5.

that the reduction of phosphorus to phosphides is kinetically preferred over PO_4^{3-}, this unexpected result requires some experimental confirmation.[33]

The garnet-type oxide electrolyte LLZO has a higher chemical compatibility with oxide cathodes unlike thiophosphate electrolytes. In particular, the reaction energies of LLZO with fully lithiated NCM and LCO are effectively zero, but reactions between LLZO and half-lithiated cathodes are still thermodynamically favorable during charging (Table S3). Despite the predicted low reactivity at 0 K, chemical reactivity at the LCO/LLZO interface to form La_2CoO_4 has been observed at 973 K.[23] The high temperature reactivity and reduction of Co from 3+ to 2+ can be understood by considering oxygen loss and the associated reduction of the transition metal at high temperature as in the study of LLZO/spinel cathode interface.[73] Also, the migration of larger cations is promoted at elevated temperatures, causing the interdiffusion of Co, La, and Zr.[23] Therefore, a thermally stable coating is still needed at the LCO/LLZO interface to suppress the interdiffusion of elements during high-temperature sintering.

Ternary metal oxide coatings and polyanionic coatings generally provide a much more stable interface with oxide cathodes than sulfide electrolytes, as indicated by their small reactivity in Figure 5. In fact, some ternary metal oxide coatings have no driving force to react with oxide cathodes in both fully lithiated and half-lithiated states (e.g., $LiTaO_3$/NCM and $LiNbO_3$/LCO interfaces). Indeed, $LiNbO_3$-coated LCO and LMO have been used effectively in SSBs with a sulfide SSE.[20,41] In contrast, phosphates-based coatings are predicted to exhibit higher reactivity with oxide cathodes (except for LFPO) than oxide coatings, which is largely driven by the tendency to form Li_3PO_4 (Table S4). Specifically, meta-phosphates containing the PO_3^- group want to obtain O from oxide cathodes to form the PO_4^{3-} group. Even for the ortho-phosphate $LiTi_2(PO_4)_3$, which already contains the PO_4^{3-} group, it is energetically favorable to give up transition-metal elements and obtain Li from the cathode to form the Li_3PO_4 phase. However, the formation of Li_3PO_4 may not

Please cite this article in press as: Xiao et al., Computational Screening of Cathode Coatings for Solid-State Batteries, Joule (2019), https://doi.org/10.1016/j.joule.2019.02.006

always be detrimental, as it has been used as a cathode coating and thin-film solid electrolyte.[38,74,75] Crystalline Li_3PO_4 possesses a reasonably high oxidation limit (4.22 V) and chemical stability, as shown in Table S1, and in partially crystalline form its ionic conductivity (σ_{RT} = $\sim 10^{-7}$ S/cm) is only slightly lower than that of LiPON.[75] Hence, Li_3PO_4 could function as a passivation layer, restricting further reactivity. Not surprisingly, phosphate oxides are quite stable with LFPO, which can be attributed to their high similarity in P-O bonding. In fact, when phosphates were recently applied for all the components in a solid-state Li-ion battery, improved interfacial stability and cyclability was observed,[76] consistent with our computational results.

The interface between an oxide coating and a thiophosphate SSE behaves similar to an oxide cathode/SSE interface with reactivity that is often larger than 100 meV/atom, driven by the formation of Li_3PO_4 and transition metal sulfides. In contrast, many polyanionic coatings provide greatly improved compatibility with thiophosphate electrolytes ($|\Delta E_{rxt}| < 100$ meV/atom), a result we observed in the high-throughput chemical reactivity screening. Interestingly, the trend is reversed at the coating/LLZO interface. Oxide coatings show low reactivity with LLZO, while the phosphates are predicted to have a non-trivial ($|\Delta E_{rxt}| > 100$ meV/atom) reactivity with LLZO, driven by the formation of Li_3PO_4. Some polyanionic oxides other than phosphates such as $LiBa(B_3O_5)_3$ show extremely high chemical compatibility with both cathodes and thiophosphate electrolytes, indicating that all the interfaces in the cathode/coating/SSE configuration can remain intact. Other lithium borates in Table S1 such as $LiSr(B_3O_5)_3$, $LiH_2B_5O_9$, $LiCs(B_3O_5)_2$, LiB_3O_5, $Li_3B_7O_{12}$, $Li_2Al(BO_2)_5$, and $Li_4B_7O_{12}Cl$ exhibit similar low chemical reactivity. Their excellent chemical stability, in addition to their good electrochemical stability, makes borates very promising cathode coatings. There are other polyanionic compounds with zero chemical reactivity with NCM and LPS: $LiAlSiO_4$ and Li_3PO_4, although their oxidation limits (4.09 and 4.22 V) are slightly lower than that of $LiBa(B_3O_5)_3$.

Ionic and Electronic Conductivity Considerations

The ionic conductivity of a coating has been emphasized less than its stability in previous studies. However, Sakuda et al. studied the electrochemical performance of SSBs using SiO_2-coated and Li_2O-SiO_2-coated cathodes and attributed the better rate capacity of the Li_2O-SiO_2-coated cathode to the higher Li-ion conductivity of its coating.[47] Also, a recent report has shown that SSBs with Li_3BO_3-Li_2CO_3 (LBCO) cathode coating exhibit better cell performance than with Li_3BO_3 (LBO) coating, which is explained by the Li ionic conductivity of LBCO, which is two orders of magnitude higher than that for LBO.[44] To evaluate and understand the ionic conductivity of the polyanionic coating candidate, we performed nudged elastic band (NEB) calculations for the single Li vacancy migration barrier. The interstitial mechanism was not considered, as interstitial Li atoms are not likely to survive at high voltage. We also did not include the vacancy formation energy in the migration barrier, as we expect that a coating layer of nanometer thickness prepared using common coating methods would be highly defective and contain intrinsic vacancies. In each structure, there are multiple possible vacancy hopping pathways. The lowest migration barrier, E_m, for a pathway that percolates the supercell is provided in the third column in Table 2, with the migration pathways shown in Figure S1. The NEB migration energies for individual hopping events are also listed in Table S6. As a reference, the migration for a reported ternary metal oxide coating material, Li_2ZrO_3, was also calculated. Li_2ZrO_3 has a calculated migration barrier of 0.48 eV for Li vacancy migration, which is smaller than the 0.56 eV found for LiPON.[68,69] Among the six polyanionic oxides considered in the current study, the calculated

Please cite this article in press as: Xiao et al., Computational Screening of Cathode Coatings for Solid-State Batteries, Joule (2019), https://doi.org/10.1016/j.joule.2019.02.006

Table 2. Computed Li Vacancy Migration Barrier, Electronic Band Gap, and Experimental Conductivity Data for Li_2ZrO_3 and the Six Polyanionic Oxides

Coatings	ICSD #	Calculated Migration Barrier (eV)	Experimental Activation Energy (eV)	Experimental Ionic Conductivity (S/cm)	Kohn-Sham Band Gap (eV)	Experimental Electronic Conductivity at RT (S/cm)
Li_2ZrO_3	31941	0.48	0.5,[77] 0.68[78]	$\sim10^{-4}$ (598 K)[78]	3.99	–
LiH_2PO_4	100200	0.33	–[a]	–	6.30	–
$LiTi_2(PO_4)_3$	95979	0.42	0.47[79]	$\sim10^{-6}$ (333 K)[79]	2.26	($\sim10^{-9}$)[85]
$LiBa(B_3O_5)_3$	93013	1.96	–	–	6.20	–
$LiPO_3$	51630	0.40	1.40[82]	2.5×10^{-8} (553 K)[82]	5.60	–
$LiLa(PO_3)_4$	416877	1.39	0.92[b81]	6.35×10^{-8} (553 K)[81]	5.22	–
$LiCs(PO_3)_2$	62514	1.27	1.31[80]	$\sim10^{-8}$ (573 K)[80]	5.65	–

See also Figure S1 and Table S6.

[a]"–" means no experimental data found in the literature for the ICSD crystal structure.

[b]The experimental activation energy for $LiLa(PO_3)_4$ was re-calculated from the Arrhenius plot in Mounir et al.,[81] as the value deduced in the original paper is not consistent with its Arrhenius plot.

migration barriers in LiH_2PO_4 (0.33 eV), $LiTi_2(PO_4)$ (0.42 eV), and $LiPO_3$ (0.40 eV) are similar to or less than those of LiPON and Li_2ZrO_3, indicating that fairly good ionic conductivity can be expected in these materials. However, the compounds with the highest oxidation limits have vacancy migration barriers larger than 1 eV, such as 1.39 eV for $LiLa(PO_3)_4$ and 1.27 eV for $LiCs(PO_3)_2$, implying low room-temperature Li-ion conductivity. We also list the experimental activation energies (E_a) and ionic conductivity for Li conduction in Table 2 for reference. As observed in Table 2, the calculated migration barriers for Li_2ZrO_3, $LiTi_2(PO_4)_3$, and $LiCs(PO_3)_2$ agree fairly well with the experimentally determined activation energy for the same crystal structures.[77–80] In contrast, the experimentally determined activation energy for $LiLa(PO_3)_4$ is 0.92 eV,[81] which is considerably lower than the calculated vacancy migration energy, which may indicate that a different migration mechanism controls the measured conductivity. Although this measured activation energy for $LiLa(PO_3)_4$ is lower than the calculated migration energy, it remains prohibitively high for Li-ion migration. $LiPO_3$ is experimentally reported to have an activation energy of 1.40 eV,[82] which is 1 eV higher than the calculated migration energy. This large difference may originate from a large vacancy formation energy, a different migration mechanism, or another rate-limiting step in the experiment. However, the conductivity of $LiPO_3$ has also been shown to be enhanced by four orders of magnitude in its glass form (50 Li_2O–50 P_2O_5), with a reduced activation energy of 0.72 eV.[82] Therefore, LiH_2PO_4, $LiTi_2(PO_4)$, and $LiPO_3$ may exhibit satisfactory ionic conductivities for coating application.

As seen in the crystalline $LiLa(PO_3)_4$ and $LiPO_3$, the calculated migration energies are not always consistent with the experimentally measured values. The mismatch is expected, as we made several assumptions in our calculations: (1) the carrier formation energy is not included, (2) a vacancy migration mechanism is assumed, and (3) the migration in grain boundaries is not considered. In experiments, the measured activation energies are complicated by the factors that were neglected in the assumptions 1–3 and thus deviate from the predicted values. Additionally, the coating may be amorphous, possibly resulting in a different ionic conductivity and activation energy compared to those in the crystalline form, as is observed in $LiPO_3$. Nonetheless, our predicted migration energies can give guidance on how the compounds may perform in crystalline form.

In terms of electronic conductivity, we use the Kohn-Sham band gaps determined from DFT calculations as a rough indicator in Table 2. This is approximate, but

Please cite this article in press as: Xiao et al., Computational Screening of Cathode Coatings for Solid-State Batteries, Joule (2019), https://doi.org/10.1016/j.joule.2019.02.006

true electronic polaron calculations[83] are extremely time consuming and their quantitative accuracy can be debated. Because the band gap calculated using LDA and GGA is underestimated,[84] we used the calculated band gap values as the lower bounds for the real band gap. As observed in the sixth column in Table 2, all the coatings have relatively large band gaps above 2.2 eV, indicating low expected electronic conductivity. As a reference, the calculated band gap for a fully lithiated NCM cathode is 1.5 eV. To improve the electrochemical stability at the coating/SSE interface, the coating must have an electronic conductivity that is at least lower than that of NCM. Thus, from the band gap indicator results, all these coatings should meet this requirement. The experimentally measured electronic conductivity of $LiTi_2(PO_4)$ is approximately 10^{-9} S/cm,[85] which is much lower than that of NCM (10^{-2}–10^{-7} S/cm).[86] This result is consistent with the electronic conductivity assessment based on the DFT-calculated band gap. Therefore, all the coatings listed in Table 2 have the potential to have low electronic conductivity and meet property 4. However, as stated in the Initial Screening, when the coating contains point defects that create carriers in the valence or conduction band[53] or is in amorphous form, both of which are likely to happen during the synthesis and coating processes, it is possible that the actual electronic conductivity of these polyanionic coatings are non-negligible despite their wide Kohn-Sham band gaps.

DISCUSSION

Interface compatibility has been a well-known issue in the development of SSBs. For some SSEs such as LiPON, decomposition at high voltage leads to the formation of a SEI layer through a self-limiting reaction.[87] The phases in these SEI layers typically have extended oxidation stability and also conduct Li ions but prohibit electron transport, passivating the cathode/SSE interface.[30,31] For other SSEs, such as sulfides, the interfacial resistance continues to grow upon cycling, causing rapid capacity fade.[24] Coating these non-passivating systems can be viewed as creating an artificial SEI. The advantage of coating is the control over the thickness and composition of the coating. A non-artificial SEI layer results from reacting an arbitrary amount of cathode and SSE, and interdiffusion of elements can extend as far as 50 nm from the interface, impeding ion transport through the thick SEI layer.[22] In contrast, a coating layer can have a well-controlled chemistry, composition, and thickness of approximately 1–10 nm.[22,36,42,88]

Strong Bonding with O Improves Coating Stability

Polyanionic oxide coatings appear promising because of their generally high oxidation stability and smaller chemical reactivity with thiophosphate solid electrolytes. For example, in the case of phosphates, the latter is due to the fact that no O-S exchange occurs between the SSE and the coating as all phosphorus in the coating is already bonded with oxygen. On the other hand, any phosphate in contact with a readily available source of Li (such as a discharged cathode or an SSE) will still have a tendency to react, driven by the very favorable formation of Li_3PO_4.

Polyanionic oxides have a higher oxidation limit because of the covalency of oxygen with the non-metal cation in the polyanion. The breakdown of a coating at the oxidation limit likely starts by extraction of an electron and a Li ion. Because the O^{2-} states are the highest occupied state in these coating oxides, they set the oxidation limit, and electron removal from them leads to the formation of peroxides, superoxides, or possibly even O_2 gas. Strong hybridization (covalency) of these oxygen states with a main group cation pushes them down in energy and effectively protects them from oxidation. This is similar to the understanding of anion oxidation in cathode materials.[89] Table 3 demonstrates this effect by comparing the oxidation limits and

Please cite this article in press as: Xiao et al., Computational Screening of Cathode Coatings for Solid-State Batteries, Joule (2019), https://doi.org/10.1016/j.joule.2019.02.006

Table 3. Oxidation Limits and Decomposition Products for Non-polyanionic Oxides and Polyanionic Oxides with Similar Cation Chemistry

Non-polyanionic Oxides	Oxidation Limit (V)	Decomposition Products at Oxidation Limit	Polyanionic Oxides	Oxidation Limit (V)	Decomposition Products at Oxidation Limit
Li_2ZrO_3	3.44	ZrO_2, O_2	$LiZr_2(PO_4)_3$	4.52	$Zr_2P_2O_9$, ZrP_2O_7, O_2
$LiTa_3O_8$	4.09	Ta_2O_5, O_2	$Li_2Ta_2(P_2O_7)_3$	5.44	P_2O_5, $TaPO_5$, O_2
$LiCr_3O_8$	4.26	Cr_5O_{12}, O_2	$LiCrP_2O_7$	4.61	$Cr(PO_3)_3$, $CrPO_4$, O_2

decomposition products for six non-polyanionic oxides and polyanionic oxides with similar cation chemistry. It can be observed that oxygen anions are oxidized at high voltage to form O_2 gas, similar to the O_2 loss observed at the surface of the cathode upon the first charge.[90,91] Polyanionic oxides, however, exhibit significantly higher oxidation limits than their non-polyanionic oxide counterparts.

We further explored the class of phosphate compounds to determine the correlation between the nature of bonding and oxidation limits. Figure 6 presents a violin plot of the distribution of the oxidation limit for the 150 phosphates that pass the phase stability filter (filter 2). They can be categorized into ortho-phosphates (31), pyro-phosphates (23), and meta-phosphates (96). In general, the PO_3^- group in the meta-phosphates exhibits the highest oxidation limits, followed by the pyro-phosphates with the $P_2O_7^{4-}$ group. Ortho-phosphates with the PO_4^{3-} group possess the lowest median oxidation limit among all the phosphates. Condensation of the polyhedral units decreases the O/P ratio in the sequence PO_4^{3-}, $P_2O_7^{4-}$, PO_3^- and enhances the hybridization of each O with P, thereby increasing the oxidation limit. This phenomenon is reminiscent of the increase of intercalation voltage in phosphate cathodes with decreasing O/P ratio due to the inductive effect.[92] In fact, both the increase of oxidation limit and the intercalation voltage can be attributed to the enhanced covalency in P-O bonding during phosphate condensation.[93]

This hybridization protection of oxygen can, to some extent, also be observed in the high oxidation limits of $LiNbO_3$ and $LiTaO_3$ oxide coatings. As 4d and 5d early transition metals, Nb and Ta have less contracted d orbitals than later transition metals or 3d transition metals, providing good hybridization for the oxygen states in these materials. While these oxides do not have an oxidation limit as high as some of the phosphate coatings, they have the benefit of very low reactivity with many oxide cathodes, as no Li_3PO_4 formation is possible. As such, they may be an excellent compromise when high-temperature operations are needed to create the coated cathode materials or to process them in a device. Unfortunately, with thiophosphate SSEs, there will be some driving force for $LiNbO_3$ and $LiTaO_3$ to exchange S and O and produce PO_4 groups. However, they are expected to be ideal as a buffer layer between LLZO and oxide cathodes if they can be kinetically stabilized at high voltage (Figure 5).

Lithium borates form an interesting and fairly unexplored alternative to phosphate coatings. The recent application of LBO and LBCO as cathode coatings has shown potential for interfacial protection.[44] Similar to phosphorus, boron provides oxygen with substantial oxidation protection through strong hybridization. Therefore, the borate in our down-selected list has very low reactivity with both cathodes and SSEs, likely due to the even stronger B-O bonds than P-O bonds, as indicated by their bond dissociation energies (597 kJ/mol for P-O bond versus 806 kJ/mol for B-O bond).[72]

Trade-off between Ionic Conductivity and Oxidation Stability

Despite the high electrochemical stability of polyanionic oxides, we note that there is a trade-off between a high ionic conductivity and a high oxidation limit in these

Please cite this article in press as: Xiao et al., Computational Screening of Cathode Coatings for Solid-State Batteries, Joule (2019), https://doi.org/10.1016/j.joule.2019.02.006

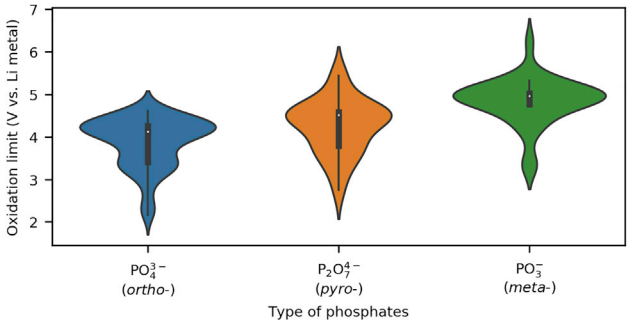

Figure 6. Distribution of Oxidation Limit for Ortho-phosphates (PO_4^{3-}), Pyro-phosphates ($P_2O_7^{4-}$), and Meta-Phosphates (PO_3^-) That Pass the Phase Stability Filter (Filter 2)

The violin plot shows the kernel density estimation of the distribution, and the inner box spans the interquartile range (IQR) of the distribution, with the whiskers extending the box by 1.5 × IQR on both sides. The white dot inside the box denotes the median.

materials. For example, $LiCs(PO_3)_2$ exhibits an extremely high oxidation limit of 6.2 V; however, its high Li-ion migration barrier (1.27 eV) may prevent its use as a cathode coating. The same problem also exists for $LiBa(B_3O_5)_3$ and $LiLa(PO_3)_4$, as observed in Table 2, and other phosphates with high oxidation limits shown in Table S1, such as $LiGd(PO_3)_4$ (V_{ox} = 5.30 V, E_a = 0.96 eV[94]), $LiK(PO_3)_2$ (V_{ox} = 5.09 V, E_a = 1.89 eV[80]), and $LiDy(PO_3)_4$ (V_{ox} = 4.86 V, E_a = 0.96 eV[95]). The trade-off can be understood by considering the correlation between the oxidation limit and Li content in the material. Figure 7A shows the oxidation limits of all 411 Li-containing polyanionic oxides that pass the phase stability filter (filter 2) as a function of their Li atomic fraction (i.e., the ratio of the number of Li atoms to the total number of atoms in the chemical formula). From the blue trend line calculated by the linear fitting of the data points in Figure 7A, it can be observed that, in general, the oxidation limit decreases with increasing Li fraction for polyanionic oxides. Figure 7B is a plot of the maximum Li fraction as a function of oxidation limit for polyanion oxides passing filter 2. For example, the point marked by "$LiPO_3$" in Figure 7B has coordinates (5 V, 0.20), meaning that for polyanionic oxides an oxidation limit of 5 V or higher can only be observed in compounds with a Li atomic fraction no greater than 0.20. Figure 7B shows that the maximum Li fraction decreases drastically at an oxidation limit above 4 V. The low Li fraction in turn indicates a large Li-Li distance and/or low Li-Li coordination number in the material. Both of these factors were observed to be negatively correlated to ionic conductivity in a recent statistical learning study of Li-ion conductors.[96] The decreased oxidation limit as the Li content increases may simply be a consequence of the fact that the chemical potential of Li tends to increase as more Li is present in a material. However, it is also likely related to the fact that Li removal from a stoichiometry is accompanied by oxygen removal, which in the case of phosphates correlates with the condensation of PO_4^{3-} units. The condensation in turn increases the oxygen covalency, as previously argued. On the other hand, although Figure 7B indicates that high oxidation stability can only be achieved in low Li-fraction polyanionic oxides, it is certainly possible that a large overpotential required for O_2 gas evolution (as is the case for LLZO[56]) enables higher Li-fraction compounds to be kinetically stabilized at a given voltage. For example, if Li_3PO_4 (V_{ox} = 4.22 V) is kinetically stabilized at 5 V, the limit of Li fraction would increase from 0.20 (in $LiPO_3$) to 0.38 (in Li_3PO_4) at that voltage.

In Figure 7A, we also highlight in red the 66 polyanionic oxides that pass the chemical reactivity screening (filter 5), 25 of which have an oxidation limit $\geq$4.5 V (green dashed line). Among the 25 compounds, $LiPO_3$ has the highest Li atomic fraction of

Please cite this article in press as: Xiao et al., Computational Screening of Cathode Coatings for Solid-State Batteries, Joule (2019), https://doi.org/10.1016/j.joule.2019.02.006

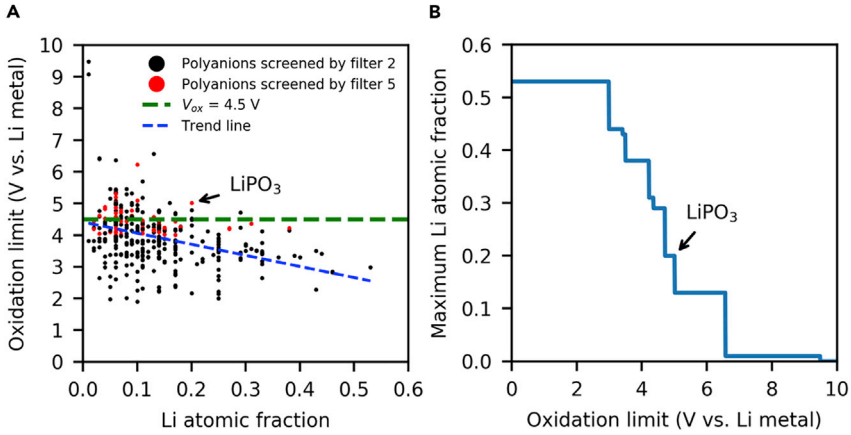

Figure 7. Correlation between Oxidation Limit and Li Atomic Fraction in Polyanionic Oxides

(A) Oxidation limit versus Li atomic fraction for the 411 polyanionic oxides (polyanions) that pass the phase stability screening (filter 2). The red dots denote the 66 polyanionic oxides that pass chemical stability screening (filter 5). The green dashed horizontal line marks the oxidation limit = 4.5 V versus Li metal. The blue dashed line is the linear trend line.

(B) Maximum Li atomic fraction versus oxidation limit for the 411 polyanionic oxides that pass the phase stability screening (filter 2). A point (*x* and *y*) in the profile means that all polyanionic oxides with an oxidation limit of *x* or higher have a maximum Li atomic fraction of *y*. $LiPO_3$ is marked by the black arrows.

20%. The resulting small Li-Li hopping distance in $LiPO_3$ contributes to the low calculated activation energy for Li vacancy migration of 0.4 eV in crystalline form and 0.72 eV measured in glassy form.[82] Therefore, $LiPO_3$ combines the advantages of excellent high voltage stability (5 V) and a low migration barrier. In fact, the use of $LiPO_3$ on the high-voltage cathode $LiNi_{0.5}Mn_{1.5}O_4$ has been demonstrated to enhance the rate performance and cyclability in a liquid electrolyte cell.[88] For cathodes with a cut-off voltage lower than 4.5 V (e.g., NCM and LCO), the electrochemical stability requirement is less stringent. In this case, we expect that using LiH_2PO_4 or $LiTi_2(PO_4)_3$ with an oxidation limit of 4.6 V as a cathode coating can also result in good cell performance. Indeed, when charged to 4.6 V, $LiTi_2(PO_4)_3$ coating enhanced the capacity retention and rate capacity of a $Li_{1.5}Ni_{0.25}Mn_{0.75}O_{2+\delta}$ cathode in a conventional Li-ion battery.[60]

Challenges with the Current Coating Strategy

Beyond the screening requirements used in this work, there are many other challenges associated with designing an optimal cathode composite. For example, the formation of electronically conductive interphase products at the coating/electrolyte interface would make the coating a mixed conductor and compromise its functionality. At the coating/sulfide interface, there is a driving force for the transition metals to form transition metal sulfides and Li transition metal sulfides as reaction products. These transition metal sulfides typically have non-negligible electronic conductivity.[97–99] Thus, to further optimize the coating composition, the transition metal content in cathode-coating materials should be reduced. In this sense, LiH_2PO_4 and $LiPO_3$ are better choices than $LiTi_2(PO_4)_3$ when paired with sulfide electrolytes. On the other hand, LiH_2PO_4 may potentially produce H_2O and H_2S gas at the interfaces with some oxides and sulfides, respectively (Tables S4 and S5). However, we expect the amount of these to be small given that the other products are passivating. These volatile products could be removed in the pre-treatment procedures such as annealing, sintering or hot-pressing, and vacuum drying. Another side reaction may be that LiH_2PO_4 exchanges protons with Li ions in LCO (or

Please cite this article in press as: Xiao et al., Computational Screening of Cathode Coatings for Solid-State Batteries, Joule (2019), https://doi.org/10.1016/j.joule.2019.02.006

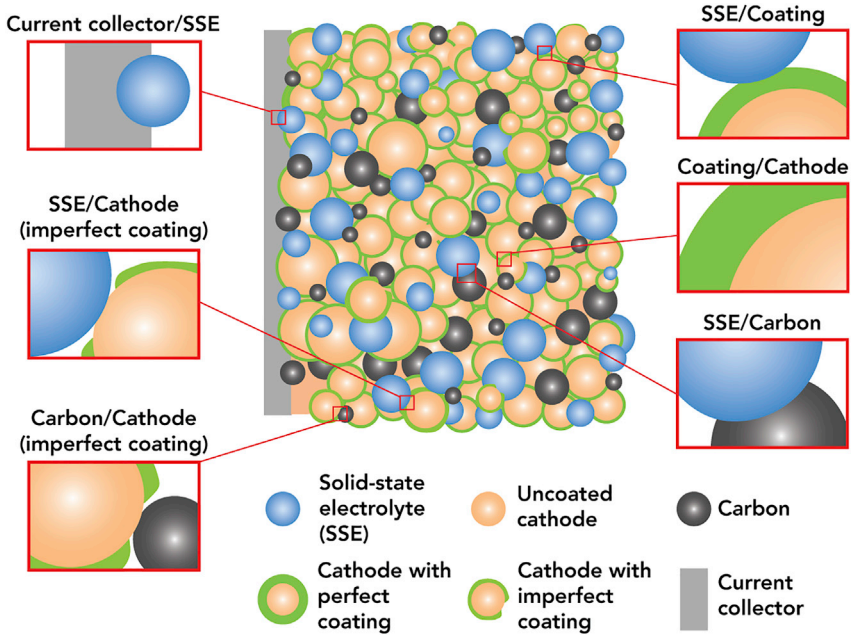

Figure 8. Various Interfaces in a Coated Cathode Composite

The general coating strategy only considers the SSE/coating and coating/cathode interfaces, whereas materials decomposition under electrochemical cycling can still occur at other interfaces, i.e., the current collector/SSE, SSE/cathode (imperfect coating), and SSE/carbon interfaces.

NCM), forming H-inserted CoO_2 ($HCoO_2$) and Li_3PO_4 (Table S4). According to the data in Table S2, this exchange reaction is thermodynamically favored with a driving force around 60 meV/atom. The fact that both proton[100] and Li^+ have good mobility in LiH_2PO_4 may facilitate the reaction at room temperature. For spinel LMO cathode, a similar exchange reaction to form H-inserted Mn_2O_4 (HMn_2O_4) and Li_3PO_4 has a small driving force (4 meV/atom), while for olivine LFPO cathode the exchange reaction to form H-inserted $FePO_4$ ($HFePO_4$) and Li_3PO_4 is not thermodynamically favorable.

Furthermore, despite the improved performance when applying a cathode coating, there is an inherent paradox of the general cathode-coating strategy: a perfect coating that stabilizes the solid electrolyte from oxidation must be electronically isolating; however, the lack of electronic conductivity in the coating would completely prevent active material redox. This phenomenon can be observed in coatings that are too thick and prevent appropriate cycling.[101] This paradox suggests that coatings either should still allow some level of free electron transport or should be imperfect, allowing the exposed surfaces of the cathode particles to form percolating electronic conduction pathways with the electronically conductive additive and current collector. Figure 8 presents a schematic illustration of a coated cathode composite with various interfaces highlighted. Although an imperfect coating would allow contact of the cathode and carbon, it also opens the door for the exposed part of the cathode to contact with the electrolyte, possibly contributing to the observed continuous impedance growth and capacity fade even in cells with a cathode coating.[39,45] Ultimately, to resolve this paradox, an improved morphological design of the different components in the composite cathode might be needed.

Another issue is the oxidation of the SSE at the interfaces with the conductive additive (e.g., carbon) and current collector, where the electrolyte is subject to the full

Please cite this article in press as: Xiao et al., Computational Screening of Cathode Coatings for Solid-State Batteries, Joule (2019), https://doi.org/10.1016/j.joule.2019.02.006

cathode voltage (Figure 8). As a result, thiophosphate decomposition is unavoidable when using a strategy of only coating the cathode, and degradation at these interfaces will form ionically insulating "dead space" in electrolyte particles.[25,27] In principle, because neither electron transfer nor Li-ion transfer is required at these interfaces, the decomposition of thiophosphates should not immediately affect the low-rate cell performance. However, "dead space" will negatively affect the ionic conductivity of thiophosphate particles and therefore increase the internal resistance of the cell. Thus far, the extent of this "dead space" effect remains unknown.

Application of coatings to a cathode can lead to either an amorphous[40,41] or crystalline form on the cathode surface. Although our studies focused on crystalline compounds, we expect the chemical and electrochemical stability to be similar to their amorphous counterparts. As discussed before in the case of $LiPO_3$, the ionic conductivity may, however, be different. In fact, in some coatings such as $LiNbO_3$, amorphous coatings exhibit higher ionic conductivity than their crystalline counterparts.[102] We note that both the six polyanionic oxides considered in the current study and the other polyanionic oxides in Table S1 mostly consist of phosphates and borates, and in these materials, favorable Li-ion conduction has been reported for their glassy form.[103,104]

Coating Selection Is Dependent on the Cathode, the SSE, and the Processing Conditions

From our results, it is clear that the choice of a coating material needs to be carefully tuned to a specific SSE/cathode combination. For example, Li_2ZrO_3 has the best chemical compatibility at the LMO/LLZO interface among all oxide coatings, whereas the lithium borate is the most stable chemistry for cathode/thiophosphate interfaces (Figure 5). It should also be expected that the choice of coating is dependent on the processing techniques that will be used to create the SSB. For example, if high-temperature sintering is required to integrate the SSE and cathode particles,[105] then the chemical stability at cathode/coating and SSE/coating may be an overriding concern, as interdiffusion of elements is accelerated at elevated temperature.[23,35] If batteries are cold-formed (e.g., by pressing) or subject to mild thermal treatment, then electrochemical stability and Li ionic conductivity may be more important issues.[24]

Finally, we make recommendations for coating materials in Figure 9 for various cathode/SSE interfaces under different processing conditions (sintering, hot-pressing, or cold-pressing). Lithium borates are recommended for all interfaces because many compounds in this category show excellent chemical stability and high oxidation limits as shown in Table S1. Although our NEB result indicates that $LiBa(B_3O_5)_3$ has a high migration barrier for lithium ion conduction, it is possible that other borates with higher Li content exhibit reasonable ionic conductivity. Phosphate coatings are recommended to be paired with sulfide SSEs but not with LLZO because their reactivity with LLZO is high and processing LLZO incurs high temperature. On the contrary, oxide coatings such as $LiNbO_3$ and $LiTaO_3$ are recommended for pairing with LLZO; with sulfide SSEs they are not optimal because of the high chemical reactivity. As shown before, oxide coatings featured a remarkable chemical stability with oxide cathodes, although at high voltage they are electrochemically metastable. Thus, the charging voltage of oxide cathodes may need to be limited when coated with these oxide coatings.

Conclusions

In summary, we have developed a computational framework to search for cathode coatings in a high-throughput manner. Phase stability, electrochemical stability,

Please cite this article in press as: Xiao et al., Computational Screening of Cathode Coatings for Solid-State Batteries, Joule (2019), https://doi.org/10.1016/j.joule.2019.02.006

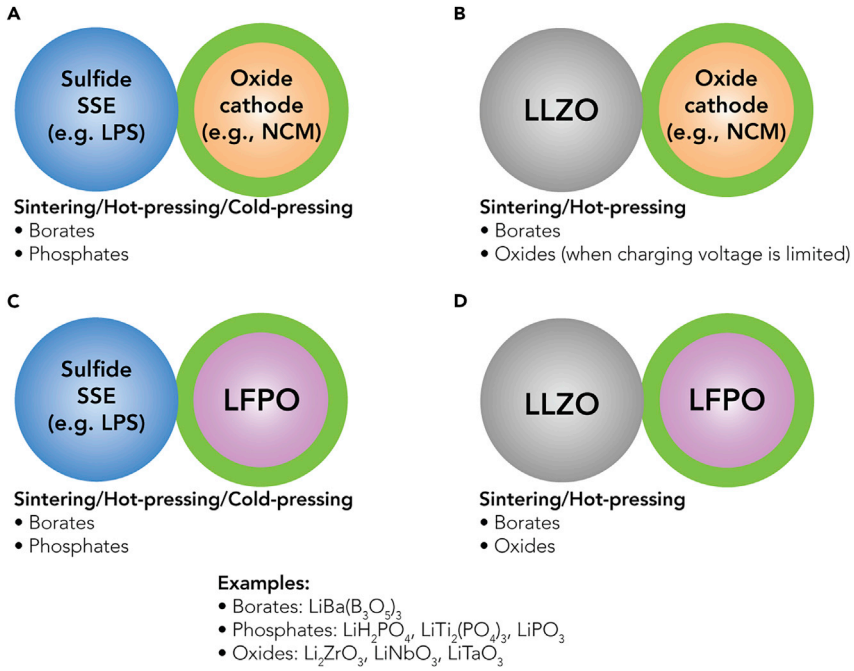

Figure 9. Coating Recommendations for Various Cathode/SSE Interfaces under Different Processing Conditions

(A) Oxide cathode/sulfide SSE. (B) Oxide cathode/LLZO. (C) LFPO/sulfide SSE. (D) LFPO/LLZO.

chemical reactivity, and ionic and electronic conductivity were used as screening criteria, and the following trends were observed: (1) because of the high covalency of oxygen, polyanionic oxides have higher oxidation limits and lower reactivity with thiophosphate electrolytes than conventional ternary metal oxide coatings and (2) in general, there is a trade-off between oxidation stability and ionic conductivity in Li-containing polyanionic oxides. Although a high oxidation limit indicates a low Li content in the compound, a high ionic conductivity is correlated to a high Li content.

Six polyanionic oxide coatings were examined in greater detail. Lithium borates such as $LiBa(B_3O_5)_3$ possess excellent electrochemical and chemical stability but may suffer from poor ionic conductivity at low Li content. Furthermore, three phosphate compounds LiH_2PO_4, $LiTi_2(PO_4)_3$, and $LiPO_3$ with good overall characteristics are highlighted for their superior properties as cathode-coating materials in SSBs. Based on the results from high-throughput screening and detailed case studies, we make specific recommendations of coating materials for various cathode/SSE interfaces.

EXPERIMENTAL PROCEDURES

First-Principles Calculations of Bulk Energies and Band Gaps

To calculate the bulk energies and Kohn-Sham band gaps of crystalline materials in the database, we used DFT within the projector augmented wave (PAW) formalism,[106] as implemented in the Vienna *ab initio* simulation package (VASP).[107] For the exchange-correlational functional, we employ a mixed scheme of the generalized gradient approximation (GGA)[108] and GGA with the rotationally invariant Hubbard (+U) correction,[109,110] as described in previous work by Jain et al.[111] An energy cut-off of 520 eV and a k-point grid of at least $500/n_{atom}$ was used for all the calculations. Similar datasets are available online as part of the Materials Project.[112]

Please cite this article in press as: Xiao et al., Computational Screening of Cathode Coatings for Solid-State Batteries, Joule (2019), https://doi.org/10.1016/j.joule.2019.02.006

Phase Stability Evaluation

The phase stability of each material was evaluated by computing the lower energy convex hull and corresponding canonical phase diagram at 0 K formed by the ground-state phases in the chemical space defined by all the elements in the material. To construct the convex hull and the canonical phase diagram, all known crystalline materials in the chemical space were included and processed using the Pymatgen software package.[113] As a result, materials with an energy above the convex hull are expected to decompose into its nearest phase on the convex hull, as this decomposition would lower the total energy of the system. The nearest phases are uniquely defined as the phases that determine the Gibbs triangle (the low-energy facet), which contains the desired composition in the phase diagram. In contrast, materials with an energy exactly on the convex hull are thermodynamically stable against decomposition and therefore pass the phase stability filter. Note that in this work, materials with energies < 0.005 eV/atom above the convex hull also pass the phase stability filter, as they are considered to be stable within DFT or temperature error.

Electrochemical Stability Window Calculation

The calculation of the electrochemical stability window follows the methodology used in the earlier work.[18,30,35] For any lithium chemical potential μ_{Li}, we consider the grand potential Φ of a compound using Equation 1, where c is the composition of the material, $E[c]$ is the enthalpy, and $n_{Li}[c]$ is the Li concentration of composition c.

$$\Phi[c, \mu_{Li}] = E[c] - n_{Li}[c]\mu_{Li} \quad \text{(Equation 1)}$$

For the stability and reaction energy calculations, materials that are metastable (e.g., $Li_{10}GeP_2S_{12}$) are placed exactly on the convex hull to account for the change in free energy when temperature is increased from 0 K to elevated temperature. Similar to using the DFT energy to construct the energy convex hull and canonical phase diagram, one can use the grand potential of materials at given lithium chemical potential μ_{Li} to construct the grand potential convex hull and grand potential phase diagram. The range of μ_{Li}, $[\mu_{ox}, \mu_{red}]$, over which the material is stable in the grand potential phase diagram can be converted into the electrochemical stability window $[V_{red}, V_{ox}]$ using Equations 2 and 3, where μ^0_{Li} is the Li chemical potential of Li metal and e is the elementary charge.

$$V_{red} = \frac{\left(\mu^0_{Li} - \mu_{red}\right)}{e} \quad \text{(Equation 2)}$$

$$V_{ox} = \frac{\left(\mu^0_{Li} - \mu_{ox}\right)}{e} \quad \text{(Equation 3)}$$

Chemical Mixing Reaction Energy

The calculation of the chemical reaction energy at the solid/solid interfaces (cathode/SSE, cathode/coating, and SSE/coating) followed the methodology used by Richards et al.[30] For two crystalline reactants A and B, the reaction energy ΔE_{rxt} was determined by considering the mixing ratio x that yielded the largest reaction driving force according to Equation 4, where c_a and c_b are the compositions of reactants A and B normalized by their numbers of atoms, respectively; $E_{pd}[c]$ is the energy of the ground-state structure or phase equilibrium at composition c determined from the convex hull. Note that ΔE_{rxt} has the unit of eV/atom or meV/atom as it is normalized by the number of atoms in the reaction.

$$\Delta E_{rxt} = min_{x\in[0,1]}\left\{E_{pd}[xc_a + (1-x)c_b] - xE[c_a] - (1-x)E[c_b]\right\} \quad \text{(Equation 4)}$$

NEB Calculations

To study the Li-ion diffusion in the coatings, we performed climbing-image NEB calculations[114,115] for the single-vacancy migration mechanism. For each material, we only considered the crystal structure with the lowest energy in the database. The vacancy was created by removing one Li ion from the pristine structure, and the defect charge was compensated by a uniform background charge to retain the oxidation state for all ions. An energy cut-off of 400 eV was used for all the NEB calculations.

SUPPLEMENTAL INFORMATION

Supplemental Information can be found online with this article at https://doi.org/10.1016/j.joule.2019.02.006.

ACKNOWLEDGMENTS

This work was primarily funded by the Samsung Advanced Institute of Technology and additionally funded by the Materials Project Program (Grant No. KC23MP) through the U.S. Department of Energy, Office of Science, Office of Basic Energy Sciences, Materials Sciences and Engineering Division under Contract No. DE-AC02-05CH11231. This research used resources of the National Energy Research Scientific Computing Center (NERSC), a U.S. Department of Energy Office of Science User Facility operated under Contract No. DE-AC02-05CH11231. This work also used the Extreme Science and Engineering Discovery Environment (XSEDE), which is supported by National Science Foundation grant number ACI-1548562.

AUTHOR CONTRIBUTIONS

G.C. conceived and supervised the project. Y.X. and L.J.M. conducted the high-throughput screening. Y.X. and Y.W. conducted the NEB calculations. Y.X. performed the data analysis and wrote the manuscript. All authors edited the manuscript.

DECLARATION OF INTERESTS

Some of the co-authors have patents filed on some coating compositions.

Received: November 21, 2018
Revised: February 9, 2019
Accepted: February 19, 2019
Published: March 21, 2019

REFERENCES

1. Quartarone, E., and Mustarelli, P. (2011). Electrolytes for solid-state lithium rechargeable batteries: Recent advances and perspectives. Chem. Soc. Rev. *40*, 2525–2540.

2. Fan, L., Wei, S., Li, S., Li, Q., and Lu, Y. (2018). Recent progress of the solid-state electrolytes for high-energy metal-based batteries. Adv. Energy Mater. *8*, 1702657.

3. Murugan, R., Thangadurai, V., and Weppner, W. (2007). Fast lithium ion conduction in garnet-type $Li_7La_3Zr_2O_{12}$. Angew. Chem. Int. Ed. *46*, 7778–7781.

4. Ohta, S., Kobayashi, T., and Asaoka, T. (2011). High lithium ionic conductivity in the garnet-type oxide $Li_{7-X}La_3(Zr_{2-X}, Nb_X)O_{12}$ (X=0–2). J. Power Sources *196*, 3342–3345.

5. Allen, J.L., Wolfenstine, J., Rangasamy, E., and Sakamoto, J. (2012). Effect of substitution (Ta, Al, Ga) on the conductivity of $Li_7La_3Zr_2O_{12}$. J. Power Sources *206*, 315–319.

6. Khireddine, H., Fabry, P., Caneiro, A., and Bochu, B. (1997). Optimization of NASICON composition for Na^+ recognition. Sens. Actuators B Chem. *40*, 223–230.

7. Fergus, J.W. (2012). Ion transport in sodium ion conducting solid electrolytes. Solid State Ion. *227*, 102–112.

8. Aono, H., Sugimoto, E., Sadaoka, Y., Imanaka, N., and Adachi, G. (1990). Ionic conductivity of solid electrolytes based on lithium titanium phosphate. J. Electrochem. Soc. *137*, 1023–1027.

9. Arbi, K., Rojo, J.M., and Sanz, J. (2007). Lithium mobility in titanium based Nasicon $Li_{1+x}Ti_{2-x}Al_x(PO_4)_3$ and $LiTi_{2-x}Zr_x(PO_4)_3$ materials followed by NMR and impedance spectroscopy. J. Eur. Ceram. Soc. *27*, 4215–4218.

10. Fu, J. (1997). Fast Li^+ ion conducting glass-ceramics in the system Li_2O–Al_2O_3–GeO_2–P_2O_5. Solid State Ion. *104*, 191–194.

11. Yamauchi, A., Sakuda, A., Hayashi, A., and Tatsumisago, M. (2013). Preparation and ionic conductivities of $(100 - x)(0.75Li_2S \cdot 0.25P_2S_5) \cdot xLiBH_4$ glass electrolytes. J. Power Sources *244*, 707–710.

12. Seino, Y., Ota, T., Takada, K., Hayashi, A., and Tatsumisago, M. (2014). A sulphide lithium super ion conductor is superior to liquid ion conductors for use in

rechargeable batteries. Energy Environ. Sci. *7*, 627–631.

13. Kamaya, N., Homma, K., Yamakawa, Y., Hirayama, M., Kanno, R., Yonemura, M., Kamiyama, T., Kato, Y., Hama, S., Kawamoto, K., et al. (2011). A lithium superionic conductor. Nat. Mater. *10*, 682–686.

14. Whiteley, J.M., Woo, J.H., Hu, E., Nam, K.-W., and Lee, S.-H. (2014). Empowering the lithium metal battery through a silicon-based superionic conductor. J. Electrochem. Soc. *161*, A1812–A1817.

15. Kuhn, A., Gerbig, O., Zhu, C., Falkenberg, F., Maier, J., and Lotsch, B.V. (2014). A new ultrafast superionic Li-conductor: Ion dynamics in $Li_{11}Si_2PS_{12}$ and comparison with other tetragonal LGPS-type electrolytes. Phys. Chem. Chem. Phys. *16*, 14669–14674.

16. Bron, P., Johansson, S., Zick, K., Schmedt auf der Günne, J., Dehnen, S., and Roling, B. (2013). Li10SnP2S12: An affordable lithium superionic conductor. J. Am. Chem. Soc. *135*, 15694–15697.

17. Kato, Y., Hori, S., Saito, T., Suzuki, K., Hirayama, M., Mitsui, A., Yonemura, M., Iba, H., and Kanno, R. (2016). High-power all-solid-state batteries using sulfide superionic conductors. Nat. Energy *1*, 16030.

18. Ong, S.P., Mo, Y., Richards, W.D., Miara, L., Lee, H.S., and Ceder, G. (2013). Phase stability, electrochemical stability and ionic conductivity of the $Li_{10\pm1}MP_2X_{12}$(M = Ge, Si, Sn, Al or P, and X = O, S or Se) family of superionic conductors. Energy Environ. Sci. *6*, 148–156.

19. Qin, S., Zhu, X., Jiang, Y., Ling, M., Hu, Z., and Zhu, J. (2018). Growth of self-textured Ga3+-substituted Li7La3Zr2O12 ceramics by solid state reaction and their significant enhancement in ionic conductivity. Appl. Phys. Lett. *112*, 113901.

20. Takada, K., Ohta, N., Zhang, L., Xu, X., Hang, B.T., Ohnishi, T., Osada, M., and Sasaki, T. (2012). Interfacial phenomena in solid-state lithium battery with sulfide solid electrolyte. Solid State Ion. *225*, 594–597.

21. Takada, K. (2013). Progress and prospective of solid-state lithium batteries. Acta Mater. *61*, 759–770.

22. Sakuda, A., Hayashi, A., and Tatsumisago, M. (2010). Interfacial observation between $LiCoO_2$ electrode and Li_2S-P_2S_5 solid electrolytes of all-solid-state lithium secondary batteries using transmission electron microscopy. Chem. Mater. *22*, 949–956.

23. Kim, K.H., Iriyama, Y., Yamamoto, K., Kumazaki, S., Asaka, T., Tanabe, K., Fisher, C.A.J., Hirayama, T., Murugan, R., and Ogumi, Z. (2011). Characterization of the interface between $LiCoO_2$ and $Li_7La_3Zr_2O_{12}$ in an all-solid-state rechargeable lithium battery. J. Power Sources *196*, 764–767.

24. Koerver, R., Aygün, I., Leichtweiß, T., Dietrich, C., Zhang, W., Binder, J.O., Hartmann, P., Zeier, W.G., and Janek, J. (2017). Capacity fade in solid-state batteries: Interphase formation and chemomechanical processes in nickel-rich layered oxide cathodes and lithium thiophosphate solid electrolytes. Chem. Mater. *29*, 5574–5582.

25. Hakari, T., Deguchi, M., Mitsuhara, K., Ohta, T., Saito, K., Orikasa, Y., Uchimoto, Y., Kowada, Y., Hayashi, A., and Tatsumisago, M. (2017). Structural and electronic-state changes of a sulfide solid electrolyte during the Li deinsertion–insertion processes. Chem. Mater. *29*, 4768–4774.

26. Zhang, W., Leichtweiß, T., Culver, S.P., Koerver, R., Das, D., Weber, D.A., Zeier, W.G., and Janek, J. (2017). The detrimental effects of carbon additives in $Li_{10}GeP_2S_{12}$-based solid-state batteries. ACS Appl. Mater. Interfaces *9*, 35888–35896.

27. Yoon, K., Kim, J.J., Seong, W.M., Lee, M.H., and Kang, K. (2018). Investigation on the interface between $Li_{10}GeP_2S_{12}$ electrolyte and carbon conductive agents in all-solid-state lithium battery. Sci. Rep. *8*, 8066.

28. Han, X., Gong, Y., Fu, K., He, X., Hitz, G.T., Dai, J., Pearse, A., Liu, B., Wang, H., Rubloff, G., et al. (2017). Negating interfacial impedance in garnet-based solid-state Li metal batteries. Nat. Mater. *16*, 572–579.

29. Mo, Y., Ong, S.P., and Ceder, G. (2012). First principles study of the $Li_{10}GeP_2S_{12}$ lithium super ionic conductor material. Chem. Mater. *24*, 15–17.

30. Richards, W.D., Miara, L.J., Wang, Y., Kim, J.C., and Ceder, G. (2016). Interface stability in solid-state batteries. Chem. Mater. *28*, 266–273.

31. Zhu, Y., He, X., and Mo, Y. (2015). Origin of outstanding stability in the lithium solid electrolyte materials: insights from thermodynamic analyses based on first-principles calculations. ACS Appl. Mater. Interfaces *7*, 23685–23693.

32. Zhu, Y., He, X., and Mo, Y. (2016). First principles study on electrochemical and chemical stability of solid electrolyte–electrode interfaces in all-solid-state Li-ion batteries. J. Mater. Chem. A *4*, 3253–3266.

33. Tang, H., Deng, Z., Lin, Z., Wang, Z., Chu, I.-H., Chen, C., Zhu, Z., Zheng, C., and Ong, S.P. (2018). Probing solid–solid interfacial reactions in all-solid-state sodium-ion batteries with first-principles calculations. Chem. Mater. *30*, 163–173.

34. Chu, I.H., Nguyen, H., Hy, S., Lin, Y.C., Wang, Z., Xu, Z., Deng, Z., Meng, Y.S., and Ong, S.P. (2016). Insights into the performance limits of the $Li_7P_3S_{11}$ superionic conductor: a combined first-principles and experimental study. ACS Appl. Mater. Interfaces *8*, 7843–7853.

35. Miara, L.J., Richards, W.D., Wang, Y.E., and Ceder, G. (2015). First-principles studies on cation dopants and electrolyte|cathode interphases for lithium garnets. Chem. Mater. *27*, 4040–4047.

36. Ohta, N., Takada, K., Zhang, L., Ma, R., Osada, M., and Sasaki, T. (2006). Enhancement of the high-rate capability of solid-state lithium batteries by nanoscale interfacial modification. Adv. Mater. *18*, 2226–2229.

37. Visco, S.J., Nimon, V.Y., Petrov, A., Pridatko, K., Goncharenko, N., Nimon, E., De Jonghe, L., Volfkovich, Y.M., and Bograchev, D.A. (2014). Aqueous and nonaqueous lithium-air batteries enabled by water-stable lithium metal electrodes. J. Solid State Electrochem. *18*, 1443–1456.

38. Takahashi, K., Hattori, K., Yamazaki, T., Takada, K., Matsuo, M., Orimo, S., Maekawa, H., and Takamura, H. (2013). All-solid-state lithium battery with $LiBH_4$ solid electrolyte. J. Power Sources *226*, 61–64.

39. Okada, K., Machida, N., Naito, M., Shigematsu, T., Ito, S., Fujiki, S., Nakano, M., and Aihara, Y. (2014). Preparation and electrochemical properties of $LiAlO_2$-coated $Li(Ni_{1/3}Mn_{1/3}Co_{1/3})O_2$ for all-solid-state batteries. Solid State Ion. *255*, 120–127.

40. Takada, K., Ohta, N., Zhang, L., Fukuda, K., Sakaguchi, I., Ma, R., Osada, M., and Sasaki, T. (2008). Interfacial modification for high-power solid-state lithium batteries. Solid State Ion. *179*, 1333–1337.

41. Ohta, N., Takada, K., Sakaguchi, I., Zhang, L., Ma, R., Fukuda, K., Osada, M., and Sasaki, T. (2007). $LiNbO_3$-coated $LiCoO_2$ as cathode material for all solid-state lithium secondary batteries. Electrochem. Commun. *9*, 1486–1490.

42. Kato, T., Hamanaka, T., Yamamoto, K., Hirayama, T., Sagane, F., Motoyama, M., and Iriyama, Y. (2014). In-situ $Li_7La_3Zr_2O_{12}$/$LiCoO_2$ interface modification for advanced all-solid-state battery. J. Power Sources *260*, 292–298.

43. Kitaura, H., Hayashi, A., Tadanaga, K., and Tatsumisago, M. (2011). Improvement of electrochemical performance of all-solid-state lithium secondary batteries by surface modification of $LiMn_2O_4$ positive electrode. Solid State Ion. *192*, 304–307.

44. Jung, S.H., Oh, K., Nam, Y.J., Oh, D.Y., Brüner, P., Kang, K., and Jung, Y.S. (2018). Li_3BO_3–Li_2CO_3: Rationally designed buffering phase for sulfide all-solid-state Li-ion batteries. Chem. Mater. *30*, 8190–8200.

45. Ito, S., Fujiki, S., Yamada, T., Aihara, Y., Park, Y., Kim, T.Y., Baek, S.-W., Lee, J.-M., Doo, S., and Machida, N. (2014). A rocking chair type all-solid-state lithium ion battery adopting Li_2O–ZrO_2 coated $LiNi_{0.8}Co_{0.15}Al_{0.05}O_2$ and a sulfide based electrolyte. J. Power Sources *248*, 943–950.

46. Aykol, M., Kim, S., Hegde, V.I., Snydacker, D., Lu, Z., Hao, S., Kirklin, S., Morgan, D., and Wolverton, C. (2016). High-throughput computational design of cathode coatings for Li-ion batteries. Nat. Commun. *7*, 13779.

47. Sakuda, A., Kitaura, H., Hayashi, A., Tadanaga, K., and Tatsumisago, M. (2008). Improvement of high-rate performance of all-solid-state lithium secondary batteries using $LiCoO_2$ coated with Li_2O–SiO_2 glasses. Electrochem. Solid-State Lett. *11*, A1–A3.

48. Rong, Z., Kitchaev, D., Canepa, P., Huang, W., and Ceder, G. (2016). An efficient algorithm for finding the minimum energy path for cation migration in ionic materials. J. Chim. Phys. *145*, 074112.

49. Jain, A., Ong, S.P., Chen, W., Medasani, B., Qu, X., Kocher, M., Brafman, M., Petretto, G., Rignanese, G.-M., Hautier, G., et al. (2015). FireWorks: a dynamic workflow system

designed for high-throughput applications. Concurr. Comput. Pract. Exp. *27*, 5037–5059.

50. Belsky, A., Hellenbrandt, M., Karen, V.L., and Luksch, P. (2002). New developments in the Inorganic Crystal Structure Database (ICSD): accessibility in support of materials research and design. Acta Crystallogr. B *58*, 364–369.

51. Hautier, G., Fischer, C.C., Jain, A., Mueller, T., and Ceder, G. (2010). Finding nature's missing ternary oxide compounds using machine learning and density functional theory. Chem. Mater. *22*, 3762–3767.

52. Green, M.A. (1990). Intrinsic concentration, effective densities of states, and effective mass in silicon. J. Appl. Phys. *67*, 2944–2954.

53. Canepa, P., Sai Gautam, G., Broberg, D., Bo, S.-H., and Ceder, G. (2017). Role of point defects in spinel Mg chalcogenide conductors. Chem. Mater. *29*, 9657–9667.

54. Kohan, A.F., Ceder, G., Morgan, D., and Van de Walle, C.G. (2000). First-principles study of native point defects in ZnO. Phys. Rev. B *61*, 15019–15027.

55. Tian, Y., Shi, T., Richards, W.D., Li, J., Kim, J.C., Bo, S., and Ceder, G. (2017). Compatibility issues between electrodes and electrolytes in solid-state batteries. Energy Environ. Sci. *10*, 1150–1166.

56. Han, F., Zhu, Y., He, X., Mo, Y., and Wang, C. (2016). Electrochemical stability of $Li_{10}GeP_2S_{12}$ and $Li_7La_3Zr_2O_{12}$ solid electrolytes. Adv. Energy Mater. *6*, 1501590.

57. Lee, S.H., Koo, B.K., Kim, J.-C., and Kim, K.M. (2008). Effect of $CO_3(PO_4)_2$ coating on Li $[Co_{0.1}Ni_{0.15}Li_{0.2}Mn_{0.55}]O_2$ cathode material for lithium rechargeable batteries. J. Power Sources *184*, 276–283.

58. Lee, H., Kim, M.G., and Cho, J. (2007). Olivine $LiCoPO_4$ phase grown $LiCoO_2$ cathode material for high density Li batteries. Electrochem. Commun. *9*, 149–154.

59. Kang, S.-H., and Thackeray, M.M. (2009). Enhancing the rate capability of high capacity $xLi_2MnO_3\cdot(1-x)LiMO_2$ (M=Mn, Ni, Co) electrodes by Li–Ni–PO_4 treatment. Electrochem. Commun. *11*, 748–751.

60. Wang, G., Wang, X., Yi, L., Wang, L., Yu, R., Liu, M., Wang, D., Ren, Q., and Yang, X. (2016). The effects of $LiTi_2(PO_4)_3$ modification on the performance of spherical $Li_{1.5}Ni_{0.25}Mn_{0.75}O_{2+\delta}$ cathode material. RSC Adv. *6*, 46325–46335.

61. Asano, T., Sakai, A., Ouchi, S., Sakaida, M., Miyazaki, A., and Hasegawa, S. (2018). Solid halide electrolytes with high lithium-ion conductivity for application in 4 V class bulk-type all-solid-state batteries. Adv. Mater. *30*, 1803075.

62. Lutz, H.D., Schmidt, W., and Haeuseler, H. (1981). Chloride spinels: A new group of solid lithium electrolytes. J. Phys. Chem. Solids *42*, 287–289.

63. Hartwig, P., Weppner, W., and Wichelhaus, W. (1979). Fast ionic lithium conduction in solid lithium nitride chloride. Mater. Res. Bull. *14*, 493–498.

64. Kanno, R., Takeda, Y., and Yamamoto, O. (1988). Structure, ionic conductivity and phase transformation of double chloride spinels. Solid State Ion. *28*, 1276–1281.

65. Martínez-Juárez, A., Pecharromán, C., Iglesias, J.E., and Rojo, J.M. (1998). Relationship between activation energy and bottleneck size for Li^+ ion conduction in NASICON materials of composition LiMM'(PO4)3; M, M' = Ge, Ti, Sn, Hf. J. Phys. Chem. B *102*, 372–375.

66. Li, Y., Zhou, W., Chen, X., Lü, X., Cui, Z., Xin, S., Xue, L., Jia, Q., and Goodenough, J.B. (2016). Mastering the interface for advanced all-solid-state lithium rechargeable batteries. Proc. Natl. Acad. Sci. USA *113*, 13313–13317.

67. Deng, Y., Eames, C., Fleutot, B., David, R., Chotard, J.N., Suard, E., Masquelier, C., and Islam, M.S. (2017). Enhancing the lithium ion conductivity in lithium superionic conductor (LISICON) solid electrolytes through a mixed polyanion effect. ACS Appl. Mater. Interfaces *9*, 7050–7058.

68. Yu, X., Bates, J.B., Jellison, G.E., and Hart, F.X. (1997). A stable thin-film lithium electrolyte: lithium phosphorus oxynitride. J. Electrochem. Soc. *144*, 524–532.

69. Hamon, Y., Douard, A., Sabary, F., Marcel, C., Vinatier, P., Pecquenard, B., and Levasseur, A. (2006). Influence of sputtering conditions on ionic conductivity of LiPON thin films. Solid State Ion. *177*, 257–261.

70. Ma, X., Kang, B., and Ceder, G. (2010). High rate micron-sized ordered $LiNi_{0.5}Mn_{1.5}O_4$. J. Electrochem. Soc. *157*, A925–A931.

71. Manthiram, A., Chemelewski, K., and Lee, E.-S. (2014). A perspective on the high-voltage $LiMn_{1.5}Ni_{0.5}O_4$ spinel cathode for lithium-ion batteries. Energy Environ. Sci. *7*, 1339–1350.

72. Dean, J.A., and Lange, N.A., eds. (1999). Lange's Handbook of Chemistry (McGraw-Hill).

73. Miara, L., Windmüller, A., Tsai, C.L., Richards, W.D., Ma, Q., Uhlenbruck, S., Guillon, O., and Ceder, G. (2016). About the compatibility between high voltage spinel cathode materials and solid oxide electrolytes as a function of temperature. ACS Appl. Mater. Interfaces *8*, 26842–26850.

74. Seki, S., Kobayashi, Y., Miyashiro, H., Mita, Y., and Iwahori, T. (2005). Fabrication of high-voltage, high-capacity all-solid-state lithium polymer secondary batteries by application of the polymer electrolyte/inorganic electrolyte composite concept. Chem. Mater *17*, 2041–2045.

75. Kuwata, N., Iwagami, N., Matsuda, Y., Tanji, Y., and Kawamura, J. (2009). Thin film batteries with Li_3PO_4 solid electrolyte fabricated by pulsed laser deposition. ECS Trans. *16*, 53–60.

76. Yu, S., Mertens, A., Tempel, H., Schierholz, R., Kungl, H., and Eichel, R.A. (2018). Monolithic all-phosphate solid-state lithium-ion battery with improved interfacial compatibility. ACS Appl. Mater. Interfaces *10*, 22264–22277.

77. Baklanova, Y.V., Arapova, I.Y., Buzlukov, A.L., Gerashenko, A.P., Verkhovskii, S.V., Mikhalev, K.N., Denisova, T.A., Shein, I.R., and Maksimova, L.G. (2013). Localization of vacancies and mobility of lithium ions in Li_2ZrO_3 as obtained by ^{6,7}Li NMR. J. Solid State Chem. *208*, 43–49.

78. Sherstobitova, E.A., Gubkin, A.F., Bobrikov, I.A., Kalashnova, A.V., and Pantyukhina, M.I. (2016). Bottle-necked ionic transport in Li_2ZrO_3: high temperature neutron diffraction and impedance spectroscopy. Electrochim. Acta *209*, 574–581.

79. París, M.A., Martínez-Juárez, A., Rojo, J.M., and Sanz, J. (1996). Lithium mobility in the NASICON-type compound $LiTi_2(PO_4)_3$ by nuclear magnetic resonance and impedance spectroscopies. J. Phys. Condens. Matter *8*, 5355–5366.

80. El Horr, N., Hammou, A., and Bagieu, M. (1991). Etude des propriétés de conduction électrique des polyphosphates: $Li_3Ba_2(PO_3)_7$, $LiPb_2(PO_3)_5$, $LiCs(PO_3)_2$, et αLiK$(PO_3)_2$. J. Solid State Chem. *90*, 361–366.

81. Mounir, F., Karima, H.-N., Khaled, B.S., and Mokhtar, F. (2012). Modeling Li-ion conductivity in $LiLa(PO_3)_4$ powder. Phys. B Condens. Matter *407*, 2593–2600.

82. Money, B.K., and Hariharan, K. (2007). Lithium ion conduction in lithium metaphosphate based systems. Appl. Phys. A *88*, 647–652.

83. Zhou, F., Kang, K., Maxisch, T., Ceder, G., and Morgan, D. (2004). The electronic structure and band gap of $LiFePO_4$ and $LiMnPO_4$. Solid State Commun. *132*, 181–186.

84. Perdew, J.P. (1985). Density functional theory and the band gap problem. Int. J. Quantum Chem. *28*, 497–523.

85. Wolfenstine, J., Allen, J.L., Sumner, J., and Sakamoto, J. (2009). Electrical and mechanical properties of hot-pressed versus sintered $LiTi_2(PO_4)_3$. Solid State Ion. *180*, 961–967.

86. Amin, R., and Chiang, Y.-M. (2016). Characterization of electronic and ionic transport in $Li_{1-x}Ni_{0.33}Mn_{0.33}Co_{0.33}O_2$ (NMC_{333}) and $Li_{1-x}Ni_{0.50}Mn_{0.20}Co_{0.30}O_2$ (NMC_{523}) as a function of Li content. J. Electrochem. Soc. *163*, A1512–A1517.

87. Schwöbel, A., Hausbrand, R., and Jaegermann, M.A.P. (2015). Interface reactions between LiPON and lithium studied by in-situ X-ray photoemission. Solid State Ion. *273*, 51–54.

88. Chong, J., Zhang, J., Xie, H., Song, X., Liu, G., Battaglia, V., Xun, S., and Wang, R. (2016). High performance $LiNi_{0.5}Mn_{1.5}O_4$ cathode material with a bi-functional coating for lithium ion batteries. RSC Adv. *6*, 19245–19251.

89. Seo, D.H., Lee, J., Urban, A., Malik, R., Kang, S., and Ceder, G. (2016). The structural and chemical origin of the oxygen redox activity in layered and cation-disordered Li-excess cathode materials. Nat. Chem. *8*, 692–697.

90. Lu, Z., and Dahn, J.R. (2002). Understanding the anomalous capacity of Li/Li[$Ni_xLi_{(1/3-2x/3)}Mn_{(2/3-x/3)}$]$O_2$ cells using in situ X-ray diffraction and electrochemical studies. J. Electrochem. Soc. *149*, A815–A822.

91. Armstrong, A.R., Holzapfel, M., Novák, P., Johnson, C.S., Kang, S.H., Thackeray, M.M., and Bruce, P.G. (2006). Demonstrating oxygen loss and associated structural reorganization in the lithium battery cathode $Li[Ni_{0.2}Li_{0.2}Mn_{0.6}]O_2$. J. Am. Chem. Soc. *128*, 8694–8698.

92. Hautier, G., Jain, A., Ong, S.P., Kang, B., Moore, C., Doe, R., and Ceder, G. (2011). Phosphates as lithium-ion battery cathodes: An evaluation based on high-throughput *ab initio* calculations. Chem. Mater. *23*, 3495–3508.

93. Padhi, A.K., Nanjundaswamy, K.S., Masquelier, C., Okada, S., and Goodenough, J.B. (1997). Effect of structure on the Fe^{3+}/Fe^{2+} redox couple in iron phosphates. J. Electrochem. Soc. *144*, 1609–1613.

94. Ettis, H., Naïli, H., and Mhiri, T. (2006). The crystal structure, thermal behaviour and ionic conductivity of a novel lithium gadolinium polyphosphate $LiGd(PO_3)_4$. J. Solid State Chem. *179*, 3107–3113.

95. Férid, M., Horchani, K., Touai, A., Madani, A., Boussetta, H., and Trabetsi-Ayedi, M. (2004). Étude des propriétés de conduction électrique des phosphates condensés mixtes éléments monovalents-terres rares: $LiDy(PO_3)_4$, $NaNd(PO_3)_4$, $AgLa(PO_3)_4$, $NH_4Dy(PO_3)_4$. J. Phys. IV Proc. *113*, 115–118.

96. Sendek, A.D., Yang, Q., Cubuk, E.D., Duerloo, K.N., Cui, Y., and Reed, E.J. (2017). Holistic computational structure screening of more than 12000 candidates for solid lithium-ion conductor materials. Energy Environ. Sci. *10*, 306–320.

97. Wagner, C. (1975). Equations for transport in solid oxides and sulfides of transition metals. Prog. Solid State Chem. *10*, 3–16.

98. Yang, J., Bao, C., Zhu, K., Yu, T., Li, F., Liu, J., Li, Z., and Zou, Z. (2014). High catalytic activity and stability of nickel sulfide and cobalt sulfide hierarchical nanospheres on the counter electrodes for dye-sensitized solar cells. Chem. Commun. *50*, 4824–4826.

99. Han, S.-C., Kim, H.-S., Song, M.-S., Kim, J.-H., Ahn, H.-J., and Lee, J.-Y. (2003). Nickel sulfide synthesized by ball milling as an attractive cathode material for rechargeable lithium batteries. J. Alloys Compd *351*, 273–278.

100. Rhimi, T., Leroy, G., Duponchel, B., Khirouni, K., Guermazi, S., and Toumi, M. (2018). AC and DC conductivity study of LiH_2PO_4 compound using impedance spectroscopy. Ionics *24*, 1305–1312.

101. Kim, H.-S., Kim, Y., Kim, S.-I., and Martin, S.W. (2006). Enhanced electrochemical properties of $LiNi_{1/3}Co_{1/3}Mn_{1/3}O_2$ cathode material by coating with $LiAlO_2$ nanoparticles. J. Power Sources *161*, 623–627.

102. Glass, A.M., Nassau, K., and Negran, T.J. (1978). Ionic conductivity of quenched alkali niobate and tantalate glasses. J. Appl. Phys. *49*, 4808–4811.

103. Martin, S.W. (1991). Ionic conduction in phosphate glasses. J. Am. Ceram. Soc. *74*, 1767–1784.

104. Tuller, H.L., Button, D.P., and Uhlmann, D.R. (1980). Fast ion transport in oxide glasses. J. Non-Cryst. Solids *40*, 93–118.

105. Ohta, S., Seki, J., Yagi, Y., Kihira, Y., Tani, T., and Asaoka, T. (2014). Co-sinterable lithium garnet-type oxide electrolyte with cathode for all-solid-state lithium ion battery. J. Power Sources *265*, 40–44.

106. Blöchl, P.E. (1994). Projector augmented-wave method. Phys. Rev. B Condens. Matter *50*, 17953–17979.

107. Kresse, G., and Furthmüller, J. (1996). Efficiency of ab-initio total energy calculations for metals and semiconductors using a plane-wave basis set. Comput. Mater. Sci. *6*, 15–50.

108. Perdew, J.P., Burke, K., and Ernzerhof, M. (1996). Generalized gradient approximation made simple. Phys. Rev. Lett. *77*, 3865–3868.

109. Anisimov, V.I., Zaanen, J., and Andersen, O.K. (1991). Band theory and Mott insulators: Hubbard U instead of Stoner I. Phys. Rev. B *44*, 943–954.

110. Dudarev, S.L., Botton, G.A., Savrasov, S.Y., Humphreys, C.J., and Sutton, A.P. (1998). Electron-energy-loss spectra and the structural stability of nickel oxide: an LSDA+U study. Phys. Rev. B *57*, 1505–1509.

111. Jain, A., Hautier, G., Ong, S.P., Moore, C.J., Fischer, C.C., Persson, K.A., and Ceder, G. (2011). Formation enthalpies by mixing GGA and GGA + U calculations. Phys. Rev. B *84*, 045115.

112. Jain, A., Ong, S.P., Hautier, G., Chen, W., Richards, W.D., Dacek, S., Cholia, S., Gunter, D., Skinner, D., Ceder, G., et al. (2013). Commentary: The Materials Project: a materials genome approach to accelerating materials innovation. APL Mater. *1*, 011002.

113. Ong, S.P., Richards, W.D., Jain, A., Hautier, G., Kocher, M., Cholia, S., Gunter, D., Chevrier, V.L., Persson, K.A., and Ceder, G. (2013). Python Materials Genomics (pymatgen): a robust, open-source python library for materials analysis. Comput. Mater. Sci. *68*, 314–319.

114. Jónsson, H., Mills, G., and Jacobsen, K.W. (1998). Nudged elastic band method for finding minimum energy paths of transitions. In Classical and Quantum Dynamics in Condensed Phase Simululations (World Scientific), pp. 385–404.

115. Henkelman, G., Uberuaga, B.P., and Jónsson, H. (2000). A climbing image nudged elastic band method for finding saddle points and minimum energy paths. J. Chem. Phys. *113*, 9901–9904.